# MATHEMATICAL PERCEPTION FOR WAINGANGA RIVER MEANDERING WITH WIDTH VARIATION

**Dr. N.L. Dongre, IPS, Ph.D., DLitt****

**It is true about the moon lit night photograph of Bajrang Ghat, Balaghat.**

***"How sweet the moonlight sleeps upon this bank!***
***Here will we sit, and let the sound of music***
***Creep in our ears: soft stillness, and the night,***
***Become the touches of sweet harmony" – By William Shakespeare***

---

**Dr. N.L. Dongre
C-14 Jaypee Nagar Rewa 486450
Email: - nl.dongre@jalindia.co.in, dongrenl@gmail.com,
Mobile No. 7869918077, 09425152076

**Abstract:-***[1] To analyze long-term evolution of meandering rivers, a mathematical modeling is applied for an efficient computation of the flow field. The estimate of the near bank velocity, required to decide the rate at which depend the outer bank migration, cannot rely on the full numerical solution of the governing equations when considering the river evolution on geological time scales. The present contribution is twofold: determining the complete linear response of a meandering river to spatially varying channel axis curvature and width, exploiting the ability of the model to describe the morphological tendencies of alluvial rivers; and developing a computationally efficient tool that can be easily incorporated in long-term plan form evolution models. The centrifugally induced secondary flow associated with channel axis curvature and longitudinal convection is accounted for by a suitable parametrization based on the structure of the three-dimensional flow field. Cross section width variations are accounted for through a suitable stretching of the transverse coordinate. The relevant momentum and mass conservation equations are then linearized by taking advantage of the fact that alluvial rivers often exhibit mild and long meander bends, as well as evident but relatively small width variations. The input data needed by the analytical solution are the spatial distribution of channel axis curvature and width variations, the mean slope of the investigated river reach, the characteristic grain size of the sediment bed and the flow discharge. The performances of the model, as well as its intrinsic limitations are discussed with reference to the comparison with the bed topography surveyed in a 41 km long reach of the Wainganga River in Balaghat,India. The results indicate that, in the presence of wide, mildly curved and long bend and weak width variations, the river topography is described with a good accuracy, thus supporting the use of the model to investigate how a river could react to changes in planform geometry or external forcing. Moreover, the analytical character of the model implies a limited computational effort, facilitating a straightforward integration within the models used to simulate the planimetric evolution of alluvial rivers on geological time scales.*

**Keyword:- Singletherd River , Wainganga River, Curuature, equilibrium, channel axis, Meandering ,Morphological tendencies.**

## 1. Introduction

[2] Alluvial rivers usually exhibit quite complex plan-forms characterized by a wide variety of alternating bends that have attracted the interest of a large number of researchers ( *Seminara* 2006, ). Much less attention has been paid to another striking feature observed in alluvial rivers (see Figure 1), namely the relatively regular spatial variations attained by the channel width. Actively meandering channels (sinuous point bar rivers) generally undergo spatial oscillations systematically correlated with channel curvature, with cross sections wider at bend apex than at crossings *[Brice,* 1975; *Hooke,* 2007]. Conversely, rivers flowing in highly vegetated flood plains, i.e., single-thread rivers, may exhibit an opposite behavior, owing to the combined effects of bank erodibility and floodplain depositional processes, which, in turn, are strictly linked to vegetation cover *[Allmendinger et al.,* 2005]. Some other streams (sinuous canaliform rivers) exhibit irregular width variations, without a clear correlation with channel curvature *[Brice,* 1975].

[3] Likewise to curvature forcing induced by bends, the presence of along channel width variations may have noticeable effects on the flow field and sediment dynamics and, thereby, on the equilibrium bed configuration *[Repetto et al.,* 2002; *Zolezzi et al.,* 2012]. Particularly, the creation of a central bar at a channel widening tends to divert the flow toward the channel banks, thus deciding erosion and widening of the river. Such enlargement, in turn, promotes sedimentation producing a subsequent narrowing and eventually, a cyclic narrowing/widening sequence[*Repetto et al,* 2002; *Hooke,* 2007; *Luchi et al.,* 2010]. The formation of a central bar is also a crucial process for understanding the dynamics of both chute cutoffs in meandering rivers *[Seminara,* 2006] and bifurcations in braided rivers *[Federici and Paola,* 2003]. The analysis carried out by *Brice* [1983] on a number of meandering streams subject to engineering realignments and relocations suggests that bend cutoff usually determines a widening of the new channel and acceleration in the growth rate of adjacent bends.

[4] A true assessment of the flow field causing from spatial distributions of channel axis curvature and cross section width, together with a physically based model simulating the outer bank erosion and the inner bank reconstruction *[Parker et al.,* 2011] are the main ingredients for developing robust

**Figure 1 (a) The Ardèche gorges are a spectacular part of France where the Ardèche river cuts through high limestone cliffs. For about 30 kilometres, the river meanders through wonderful scenery which attracts many tourists during the summer who hike, canoe, kayak and climb in the area.**

**Figure 1 (b) The typical rivers Denwa ,India exhibiting both curvature and channel width variations**

**Figure 1 (c) Wainganga River is present the reliable assessment and field observation resulting from spatial channel axis crvature.**

mathematical models that explain the morphodynamic evolution of alluvial rivers. Many attempts have been put forward to this study. Numerical *[Mosselman,* 1998; *Duan and Julien,* 2005; *Routher and Olsen,* 2007; *Darby et al.,* 2002] and semianalytical models *[Crosato,* 2007; *Chen and Duan,* 2006; *Motta et al.,* 2012] have been tested versus laboratory experiments and field data. Some of these models *[Mosselman,* 1998; *Darby et al.* , 2002; *Chen and Duan,* 2006] include also mechanistic models of bank erosion that induce width adjustments when simulating the short-term (order of years/decades) migration of a channel. Theoretical three-dimensional nonlinear models have been applied to analyze the amplitude of width variations and their phase lag with respect to channel curvature fluctuations *[Solari and Seminara,* 2005]. More recently, *Luchi et al.* [2011] investigated the effects of periodic width oscillations on bend instability, accounting for the mutual nonlinear interactions between plani-metric forcing induced by curvature and width variations. Spatial distribution of channel curvature typically determines the formation of a rhythmic bar-pool pattern strictly associated with the development of river meanders. Along channel width variations are characterized by a sequence of narrowing, yielding a central scour, alternated to the downstream development of a widening associated with the formation of a central bar. Finally, the 3-D fully nonlinear analytical model of flow and bed topography in meandering rivers developed by *Bolla Pittaluga et al.* [2009] to account for nonlinearity in sinuous mildly curved and long bends has been extended by *Luchietal.* [2012] to treat spatial variations of channel width in a sequence of sine-generated meanders. The model suggests that, for a constant longitudinal free-surface slope, the equilibrium width oscillates with a frequency twice that of the channel curvature. These periodic

oscillations are correlated with channel curvature, such that the maximum width is experienced close to inflection points while the minimum occurs close to bend apexes.

[5] In this study, a morphodynamic model that foretells, at a linear level, the spatial distribution of the flow field and the equilibrium bed configuration of an alluvial river characterized by arbitrary (in general not periodic) distributions of both the channel axis curvature and the channel width. Linear models of the steady flow in meandering channels have played a major role in disclosing a variety of features of the meandering phenomenon [ *Seminara,* 2006], in exploring the long-term (order of centuries) evolution *[Howard,* 1992; *Sun et al.,* 1996; *Frascati and Lanzoni,* 2009], and in evaluating the possible existence of a statistically universal behavior of meandering rivers *[Frascati and Lanzoni,* 2010]. A detailed comparison of the performance of different linear models can be found in *Camporeale et al.* [2007] and *Frascati and Lanzoni* [2009]. In the following, the model used by *Frascati and Lanzoni* [2009, 2010]is extended to study the morphodynamic regime and the long-term evolution of alluvial rivers, by relaxing the assumption of constant channel width. The model, owing to its analytical character, provides a computationally sustainable and robust tool that can be easily incorporated in long-term models of river planform evolution. It is also shown, through a comparison with field data, that it can be used to rapidly assess the morphological tendencies of an alluvial river in response to variations in planform geometry or hydrodynamic forcing.

[6] The rest of the paper is arranged as follows. In section 2, it is found that a two-dimensional, depth-averaged model for flow and bed topography in alluvial meandering channels with both arbitrarily differing curvature and width. Section 3 is devoted to the linearized solution of the morphodynamic problem, to brief the input data and to discuss the applicability conditions of the model. Some findings, along with a direct application of the model to a test case (a reach of the Wainganga River, India) are presented in section 4. Finally, section 5 concludes the paper drawing some conclusions

## 2. Mathematical Formulation

[7] Here the formulated mathematical model describes the steady, nonuniform flow and sediment transport in channels with arbitrarily varying curvature and not regularly variable width. The governing two-dimensional equations are derived by depth-averaging the three-dimensional conservation equations and accounting for the dynamic effects of secondary flows induced by curvature and width variation forcing. A two-parameter perturbation expansion technique, considering perturbations induced by curvature and width variations, is adopted to linearize the governing equations.

### 2.1. The Three-Dimensional Model

[8] The steady flow occurring in a meandering cohesionless channel characterized by a slowly varying distribution of both channel axis curvature $C^*(s^*)$ and half width $B^*(s^*)$. Flow and bed topography are indicated to an orthogonal intrinsic reference system ($s^*$, $n^*$, $z^*$), where $s^*$ is the longitudinal (stream wise) coordinate, $n^*$ is the lateral coordinate orthogonal to $s^*$, and $z^*$ is the vertical coordinate pointing upward (see Figure 2). Hereafter a superscript asterisk will indicate dimensional variables. In the case of channels with no uniform width, it is convenient to define the following dimensionless variables

$$\begin{gathered}(B^*, s^*) = B^*_{avg}(B, s), \qquad n^* = B^* n, \\ (u^*, v^*, w^*) = U^*_u(u, v, w/\beta_u), \\ (D^*, h^*, z^*) = D^*_u(D, F_u^2 h, z), \\ v^*_T = v_T \sqrt{C_{fu}}(U^*_u D^*_u), \\ (q^*_s, q^*_n) = \sqrt{g d^*_s}(p_s - p)/p d^*_s(q_s, q_n),\end{gathered} \tag{1}$$

where $B^*_{avg}$ is the reach averaged half width, $\mathbf{u^*} = (u^*, v^*, w^*)$ is the velocity vector (averaged over turbulence), $D^*$ is the local flow depth, $h^*$ is the free surface elevation, computed with respect to the local horizontal plane $n^*, v^*_T$ containing is the turbulent eddy viscosity, $\boldsymbol{q}^* = \left(q^*_s, q^*_n\right)$ is the sediment flux per unit width, $g$ is the acceleration due to gravity, $p$ and $p_s$ are water and sediment density, respectively,

and $d_s^*$ is sediment grain size (taken to be uniform). Furthermore, $C_{fu}$ is the friction coefficient, $\beta_u = \beta_{avg}^*/D_u^*$ is the aspect ratio of the channel, $F_u = U_u^*/\sqrt{gD_u^*}$ is the Froude number and the subscript "u" refers to properties of uniform flow in a straight channel having constant width $2B_{\mathrm{avg}}^*$ the same flow discharge and grain size of the meandering river, and a channel slope equal to the average slope in the meandering reach. A detailed discussion of how the local channel width is estimated is reported in section 3.3.

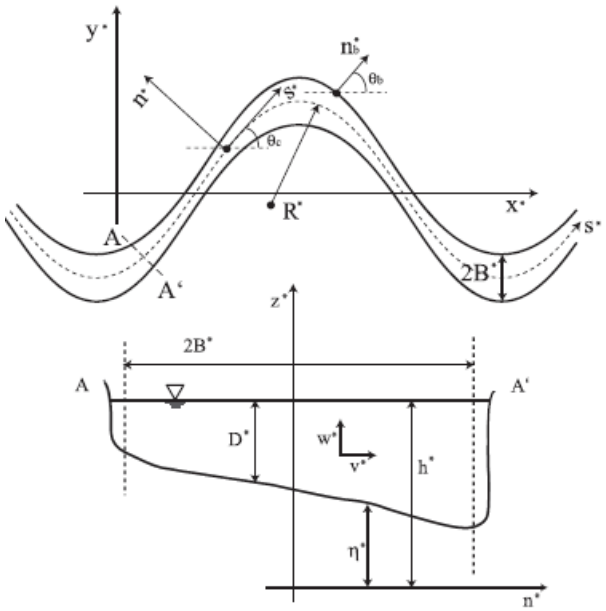


**Figure 2. Sketch of the meandering channel and notations.**

[9] The initial point of the model is supported by the steady Reynolds equations for longitudinal and transversal momentum along with the continuity equations for the fluid and solid phases. Observing that longitudinal and transverse gradients are much smaller than vertical gradients, owing to the relatively shallow depth of the flow, the dimensionless form of these equations reads as follows (see Appendix A):

$$N_u \mathcal{L}_b u + B^{-1} v u_{,n} + w u_{,z} + N_v C_u v = -N\left(\mathcal{L}_b h + \beta C_{fu}\right) + \beta_u \sqrt{C_{fu}}(v_T u_{,z}), z \tag{2}$$

$$N_u \mathcal{L}_b v + B^{-1} v v_{,n} + w u_{,z} + N_v C_{u^2} = B^{-1} h_{,n} + \beta_u \sqrt{C_{fu}}(v_T v_{,z}), z \tag{3}$$

$$N \mathcal{L}_b u + \left(N_v C + B^{-1} \frac{\partial}{\partial n}\right) v + w_{,z} = 0 \tag{4}$$

$$N \mathcal{L}_b q_s + \left(N_v C + B^{-1} \frac{\partial}{\partial n}\right) q_n = 0 \tag{5}$$

where a comma indicates partial derivative. In these equations, $C$ is the dimensionless channel axis curvature and $v$ is the curvature ratio, such that

$$v = \frac{B_{\mathrm{avg}}^*}{R_0^*}, \; C(s) = \frac{R_0^*}{R^*(s^*)} = \mathcal{O}(1) \; , \qquad \frac{\partial \theta_c}{\partial s} = -v \, C(s) \tag{6}$$

with $\theta_c$ the angle that the local tangent to the channel axis forms with the direction of an arbitrarily selected Cartesian axis of reference, $x^*$ (see Figure 2) and $R_0^*$ some characteristic value of the radius of curvature $R^*$ of the channel axis (e.g., its minimum value in the meandering reach). Furthermore, the longitudinal metric coefficient of the coordinate system, $N$, and the differential operator $\mathcal{L}_b$ are defined as follows (see Appendix A):

$$N = \frac{1}{1+vnBC} \qquad \mathcal{L}_b = \frac{\partial}{\partial s} - \frac{n}{B} B_{,s} \frac{\partial}{\partial n} \tag{7}$$

[10] Note that the operator $\mathcal{L}_b$arises as a consequence of the stretching of the coordinate $n$, which has been normalized with the local width $B^*(s^*)$ and, hence, varies in the interval ± 1. Equations (2)-(5) are associated with the following boundary and integral conditions:

$$u = v = w = 0 \ \ (z = z_0)$$
$$u_{,z} = v_{,z} = w - N\mathcal{L}_b(F_u^2 hu) - B^{-1}F_u^2 h_{,n}\, v = 0 \ (z = F_0^2 h)$$
$$\int_{Z_0}^{F_0^2 h} \mathbf{u}\,.\,\mathbf{n}_b \mathrm{d}_z = \mathrm{q}.\,\mathrm{n}_b = 0 \ (n = \pm 1)$$

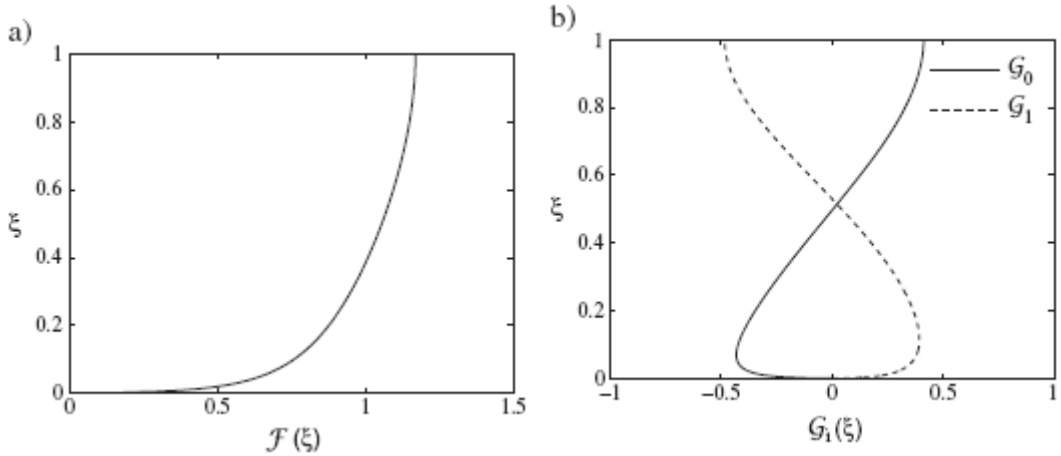


**Figure 3. (a) Vertical distribution of the function $\mathcal{F}$ describing the structure of the primary flow. (b) Vertical distribution of the functions $\mathcal{G}_0$and $\mathcal{G}_1$ describing the two components of the secondary flow. The value of the friction coefficient $C_{fu}$ has been assumed to be equal to 0.0043 (plane bed).**

where $\mathbf{n}_b$ is the unit vector locally normal to the banks. They express the no-slip condition at the bed (with $z_0$ the reference level at which this condition is imposed under uniform flow conditions); the conditions of no stress at the free surface and the requirement that the latter must be a material surface; the physical requirement that the channel walls are impermeable both to the flow and the sediment.

[11] Three further integral conditions are required in order to solve the problem. They denote the requirement that flow discharge, sediment supply, and averaged reach slope are not affected by perturbations of either the flow field or the bed configuration. These conditions will be explicitly defined in the following section.

### 2.2. A Two-Dimensional Depth-Averaged Model

[12] To derive a depth-averaged form of equations (2)-(5) that accounts for centrifugally induced secondary flow with zero average,*[Kalkwijk and De Vriend,1980: Smith and McLean, 1984; Johannesson and Parker, 1989; Zolezzi and Seminara, 2001]:*

$$u = U(s,n)\mathcal{F}(\xi)$$
$$v = v\,\bar{v}(s,n,\xi) + V(s,n)\mathcal{F}(\xi) \tag{8}$$

[13] Here $U$ and $V$ denote the depth-averaged values of $u$ and $v$, $\bar{v}$ denote the local distribution of the transverse secondary flow and $\mathcal{F}$ is a dimensionless function describing the vertical structure of the uniform flow. Furthermore, $\xi$ is a normalized vertical coordinate which reads

$$\xi = \frac{z-\left(F_u^2 h - D\right)}{D} \tag{9}$$

[14] Since the depth averages of $u$ and $v$ must, by definition, be equal to $U$ and V, from Equations (8), it follows that

$$\int_{\xi_0}^{1} \mathcal{F}(\xi)\mathrm{d}\xi = 1 \qquad \int_{\xi_0}^{1} \bar{v}\,(s,n,\xi)\mathrm{d}\xi = 0 \tag{10}$$

with $\xi_0$ the normalized reference level for no slip, a weakly dependent function of the longitudinal and lateral coordinates.

[15] The structures of the functions $\mathcal{F}$ and $\bar{v}$ are obtained following the method proposed by *Zolezzi and Seminara* [2001]. The transverse momentum equation (3), rewritten in terms of the coordinate system$(s,n,\xi,)$, is solved by means of an iterative procedure, assuming a slowly varying structure of the eddy viscosity profile of the form $v_T = UDN(\xi)$, where the vertical distribution function *N(*$\xi$) is taken to coincide with that characteristic of uniform flow, corrected through a wake function *[Dean,* 1974]. On the basis of this formulation, at the leading order of approximation $\mathcal{O}(v^0)$ the function *F(*$\xi$*)* is found to follow the classical logarithmic distribution, corrected by the wake function (Figure 3a). Moreover, from the first of the integral conditions (10), it results that $\xi_0 = \exp\left(-k/C_{fu} - 0.777\right)$, with $k$ = 0.41, the von Karman's constant.

[16] At the order $\mathcal{O}(v)$we obtain

$$\bar{v}(s,n,\xi) = \frac{DUC}{\beta_u\sqrt{C_{fu}}}\mathcal{G}_0(\xi) + \frac{D^2(UC)_{,s}}{\beta_u^2 C_{fu}}\mathcal{G}_1(\xi) \tag{11}$$

where the functions $\mathcal{G}_0(\xi)$ and $\mathcal{G}_1(\xi)$ obtained through the solutions of two second-order boundary value problems, describe the vertical structure of the secondary flow (Figure 3b). In particular, $\mathcal{G}_0$ accounts for the vertical structure of the secondary flow associated with centrifugal effects under fully developed flow conditions (i.e., not depending on s), while $\mathcal{G}_1$ is related to the phase lag between the secondary flow and the curvature induced by longitudinal convection. Note that the structure of secondary flow described by equation (11) is slightly different from that proposed by *Zolezzi and Seminara* [2001]. In fact, the function $\mathcal{G}_2(\xi)$, which appears in *Zolezzi and Seminara* [2001, equation (3.13)] turns out to be redundant if the continuity equation is used to rearrange the lateral momentum equation (3).

[17] The parametrization of the secondary flow here employed does not account for deviations of streamline curvatures with respect to that of the channel axis arising from width variations. Even though the present framework is sufficiently flexible to encompass also these deviations, the use of the above described secondary flow parametrization is nevertheless reasonable at a first-order of approximation, and it is adopted here to keep the algebraic work at the lowest level of complexity. It is discussed in Appendix B the possible effects of streamline curvature and show how, following *Repetto et al.* [2002], it can be included these effects on transverse bottom shear stress.

[18] The problem formulated so far is tackled by substituting from the decomposition (8) and the relation (11) into the differential equations (2)-(5), written in terms of the normalized variable $\xi$, and performing depth integration. At the leading order of approximation, the depth-averaged shallow-water equations governing the morphodynamics of meandering channels with variable width read

$$\left(UU_{,s} + VU_{,n}\right) + H_{,s} + \beta_u\frac{\tau_s}{D} = \delta f_{01} + v f_{10} \tag{12}$$

$$\left(UV_{,s} + VV_{,n}\right) + H_{,n} + \beta_u\frac{\tau_n}{D} = \delta \mathrm{g}_{01} + v \mathrm{g}_{10} \tag{13}$$

$$(DU)_{,s} + (DV)_{,n} = \delta m_{01} + v m_{10} \quad (14)$$

$$q_{s,s} + q_{n,n} = \delta n_{01} + v n_{10} \quad (15)$$

where the momentum correction factor $\int_{\xi_0}^{1} \mathcal{F}^2(\xi)\mathrm{d}(\xi)$ accounting for vertical velocity gradients has been assumed to be $1 \cong$. The parameter $\delta$, quantifying the intensity of width variability along the streamwise direction, is defined as

$$\delta = \frac{B_0^* - B_{avg}^*}{B_{avg}^*}, B = 1 + \delta\mathcal{B}(s), \quad (16)$$

Have denoted with $B_0^*$ some characteristic value of the half width $B^*$ of the channel (e.g., its maximum value in the meandering reach) and with $\mathcal{B} = \left(\mathcal{B}^* - B_{avg}^*\right)/\left(B_0^* - B_{avg}^*\right)$ $O(1)$quantity measuring the longitudinal variability of the width disturbances. Moreover, in equations (12)-(15),$H = \left(h - \beta_u C_{fu} s\right)$ represents the free-surface elevation with respect to a given horizontal datum.

[19] The quantities $f_{10}$, $f_{10}$, $g_{10}$, $g_{01}$, $m_{10}$, $m_{01}$, $n_{10}$,and $n_{01}$, which represent on the right-hand sides of equations (12)-(15) quantify the first-order forcing effects due to the presence of curvature and width variations. The expressions of these functions are given in Appendix C. It is sufficient to mention that they involve the coefficients

$$k_i = \int_{\xi_0}^{1} \mathcal{F}\mathcal{G}_i \mathrm{d}\xi \quad (i = 0,1) \quad (17)$$

this account for the dispersive effects due to nonlinear interactions associated with centrifugal and convective components of the secondary flow.

[20] The boundary conditions to be associated with equations (12)-(15) impose the physical requirement that channel walls are impermeable to flow and to sediment transport:

$$-UB_{,s} + V = 0, -q_s B_{,s} + q_n = 0 \ (n = \pm 1) \quad (18)$$

[21] In order to fully close the problem, additional relations are needed for determining the bed shear stress $\boldsymbol{\tau} = \left(\tau_{s,}\tau_n\right)$and the sediment flux per unit width $\mathbf{q} = \left(q_{s,}q_n\right)$ Employing the decomposition (8) and the solutions for $\mathcal{G}_0(\xi)$ and $\mathcal{G}_1(\xi)$, we find

$$\left(\tau_{s,}\tau_n\right) = C_f\sqrt{U^2 + V^2}\left(U, \tilde{V}\right) \quad (19)$$

where the quantity

$$\tilde{V} = V + v\left(\frac{DUC}{\beta_u\sqrt{C_{fu}}}k_2 + \frac{D(DUC)_{,s}}{\beta_u^2 C_{fu}}k_3\right) \quad (20)$$

accounts for centrifugal and convective secondary flows effects through the coefficients

$$k_2 = \left[\frac{\mathcal{G}_0,\xi}{\mathcal{F},\xi}\right]_{\xi_0} \quad k_3 = \left[\frac{\mathcal{G}_1,\xi}{\mathcal{F},\xi}\right]_{\xi_0} \quad (21)$$

[22] The general value of the friction coefficient *Cf* mostly depends on the bed configuration. Here it is employed that the general logarithmic formula *[Einstein,* 1950] for a plane bed, in the formula by *Engelund and Hansen* [1967] is used for a dune-covered bed.

[23] Sediment transport is assumed to be decided by local flow conditions and to deviate from the direction of the average bed stress under the action of gravity. This deviation, however, can be ignored along the longitudinal direction, owing to the very small streamwise slope usually characterizing alluvial rivers. Otherwise, the gravitational effect on the transverse direction can be accounted for following a

well-established approach of semi empirical nature, which holds for small enough values of the transverse slope *[Seminara,* 1998; *Parker et al.,* 2003]. So that

$$\left(q_{s,}q_n\right) = \Phi\left(\tau_*\colon D; R_p\right)\left(1, \frac{\tau_n}{|\tau|} - \frac{B^{-1}}{\beta_u}\frac{r}{\sqrt{\tau*}}\eta_{,n}\right) \tag{22}$$

where *r* is an empirical constant ranging about 0.5-0.6 *[Talmon et al.,* 1995], and $\eta$= *($F^2{}_u H$* - D) is the dimensionless bed elevation. Depending on the bed configuration, several empirical or semi-empirical relationships can be used to estimate the local bed load intensity, Φ, which is a monotonically increasing function of the Shields stress r* (a dimensionless form of the shear stress acting on the bed) for a given particle Reynolds number *Rp* . In the following we adopt the Meyer-Peter and Miiller formula as modified by *Wong and Parker* [2006]). Note that, at the leading order of approximation (corresponding to uniform flow conditions in a straight channel) equation (22) must satisfy the zero-divergence condition, implying that Φ is constant and equal to the uniform flow value $\Phi_u$

[24] Ultimately, the above generated problem is subject to the integral constraints stipulating which flow and sediment discharge is to be constant at any cross section, and that the averaged reach slope should not be changed by the development of perturbations by following equations:

$$\int_{-1}^{1} \mathrm{UDB}\ \mathrm{d}n = 2,\ \int_{-1}^{1} \Phi \mathrm{B}\ d\mathrm{n} = 2\Phi_u, \tag{23}$$

$$\int_0^L \int_{-1}^{1} (F_u^2 H - D)\, B\ \mathrm{d}n\mathrm{d}s = const. \tag{24}$$

having denoted with *L* the overall streamwise length of the reach under investigation.

## 3. The Linearized Form of the Problem

[25] Now it is assumed that the perturbations of uniform flow and bed topography induced by spatial variations of curvature (equation (6)) and width (equation (16)) are too enough to permit for linearization of equations (12)-(15) and (18). Looking advantage of the typically wide character of river bends and of the weakness of width variations, it is expanded that the solution in powers of the small perturbation parameters *v* and $\delta$:

$$\begin{aligned}(U, V, D, H) = (1,0,1, H_0) + \delta\left(u_{b,}v_{b,}d_{b,}h_b\right)\\ +v\left(u_{c,}v_{c,}d_{c,}h_c\right) + \cdots\end{aligned} \tag{25}$$

where,$\mathrm{H}_0 = 1 - \beta \mathrm{C}_{\mathrm{fu}}\mathrm{s}$, while$\left(u_{c,}v_{c,}d_{c,}h_c\right)$ and $\left(u_{b,}v_{b,}d_{b,}h_b\right)$ are the perturbations associated with channel axis curvature and channel width variations, respectively. To derive the differential problems governing the morphodynamics of meandering rivers with varying width, we next expand,$C_{f,}\tau_{*,}$ and Φ in the form:

$$\begin{aligned}C_f &= C_{fu}\left(1 + v\ C_{f1} + C_{f2}\right)\\ \tau_* &= \tau_{*u}(1 + v\tau_{*1} + \delta\tau_{*2})\\ \Phi &= \Phi_u(1 + v\ \Phi_1 + \delta\Phi_2)\end{aligned} \tag{26}$$

[26] The approach implicitly accepted that the friction coefficient, the Shields parameter, and the intensity of sediment transport can be evaluated in terms of local values of flow and sediment parameters, a quasi-equilibrium assumption, that is justified by the slowly varying character of both flow field and sediment dynamics. The expressions of coefficients $C_{fi,}\tau_{*i,}(i = 1,2)$are given in Appendix C.

[27] A set of perturbed equations may be obtained at every order of approximation by substituting expansions (25) and (26) into the governing 2-D equations (12)-(15) and (18). Particularly, zero order terms in the perturbation parameters *v* and $\delta$ describe the flow in a straight, uniform channel (i.e., the uniform base flow); first-order v terms define a set of equations describing the deviation of the flow field

from the uniform solution due to the channel axis curvature; first-order $\delta$ terms provide a set of equations that describe the deviation of the flow field induced by spatial variations of channel width. Higher-order terms are neglected in a linearized contest.

### 3.1. The Linear Response Forced by Width Variations

[28] The linear response of flow field and bed configuration to the forcing induced by channel width variations is described by the $\mathcal{O}(\delta)$ homogeneous linear differential problem:

$$\mathcal{L}\begin{pmatrix} u_b \\ v_b \\ d_b \\ h_b \end{pmatrix} = \begin{pmatrix} 0 \\ 0 \\ 0 \\ 0 \end{pmatrix} \tag{27}$$

with the associated nonhomogeneous boundary conditions

$$v_b = \pm B', \quad (F_u^2 h_b - d_b)_{,n} = 0 \ (n = \pm 1) \tag{28}$$

[29] Here $B'$ denotes the first derivative of width variations while $\mathcal{L}$ is the linear differential operator:

$$\mathcal{L}\begin{pmatrix} \left(\frac{\partial}{\partial_s} + \mathrm{a}_1\right) & 0 & \mathrm{a}_2 & \frac{\partial}{\partial_s} \\ 0 & \left(\mathrm{a}_1 \frac{\partial}{\partial_s} + \mathrm{a}_3\right) & 0 & \frac{\partial}{\partial_n} \\ \frac{\partial}{\partial_s} & \frac{\partial}{\partial_n} & \frac{\partial}{\partial_s} & 0 \\ \mathrm{a}_4 \frac{\partial}{\partial_s} & \frac{\partial}{\partial_n} & \left(\mathrm{a}_5 \frac{\partial}{\partial_s} + \mathrm{a}_6 \frac{\partial^2}{\partial_{n^2}}\right) & -\mathrm{a}_6 F_u^2 \frac{\partial^2}{\partial_{n^2}} \end{pmatrix} \tag{29}$$

with $a_i$ and $b_i$ $(i = 1{,}6)$ constant coeffcients reported in Appendix C.

[30] According to the theory developed by *Repetto et al.* [2002] the solution given by equations (27) and (28) denotes an extension to channels with an arbitrary width distribution of for channels with small-amplitude, sinusoidal width variations. The forcing resulted to width variations is accommodated by the boundary conditions (28).

[31] To solve in closed form the above partial differential equation problem, it is changed into a linear system of ordinary differential equations by adopting the method of separation of variables and setting:

$$u_b = u_{b0} + \sum_{m=1}^{\infty} u_{b_m} \cos(M_b n)$$

$$v_b = \overline{v_b} n + \sum_{m=1}^{\infty} u_{b_m} \sin(M_b n)$$

$$d_b = \overline{d_b} n^2 + d_{b0} + \sum_{m=1}^{\infty} d_{b_m} \cos(M_b n) \tag{30}$$

$$h_b = \bar{h}_b n^2 + h_{b0} + \sum_{m=1}^{\infty} h_{b_m} \cos(M_b n)$$

Where $M_b = m\pi$, and

$$\bar{v}_b = B'$$

$$\bar{h}_b = -\frac{1}{2}(a_3 B' + a_7 B'')$$

$$\bar{d}_b = F_u^2 \bar{h}_b \tag{31}$$

[32] Note that the Fourier expansions (30) along with conditions (31) satisfy the boundary conditions and respect the antisymmetric character of $v_b$ and the symmetric character of $u_b$, $d_b$, and $h_b$ due to width variations.

[33] By means of integral conditions (24), the $\mathcal{O}(\delta)$solution for the first Fourier mode ($m = 0$) reads

$$\begin{gathered} v_{b0} = \bar{v}_b = \mathcal{B}' \\ v_{b0} = c_1 \mathcal{B} \\ d_{b0} = c_2 \mathcal{B} - \bar{d}_b A_{b_o} \\ h_{b0} = c_1 \mathcal{B} - \bar{h}_b A_{b0} - (a_1 c_1 + a_2 c_2) \int_0^s \mathcal{B}(\bar{s})\, \mathrm{d}\bar{s} \end{gathered} \tag{32}$$

Where

$$c_1 = \frac{a_5 - 1}{a_4 - a_5} c_2 = \frac{1 - a_4}{a_4 - a_5}\ A_{b_o} = \frac{1}{3} \tag{33}$$

[34]The result for the higher lateral Fourier modes ($m > 0$)is then obtained by substituting relations (30) and(31) into equations (27) and (28), respectively. The undermentioned system of four ordinary differential equations with constant coefficients is obtained:

$$\left(\frac{\mathrm{d}^4}{\mathrm{d}s^4} + \sigma_{3_b} \frac{\mathrm{d}^3}{\mathrm{d}s^3} + \sigma_{2_b} \frac{\mathrm{d}^2}{\mathrm{d}s^2} \sigma_{1_b} \frac{\mathrm{d}}{\mathrm{d}s} + \sigma_{0_b}\right) u_{b_m} = \sum_{i=1}^{4} p_{i_b} \frac{d^i \mathcal{B}}{d_{s^i}} \tag{34}$$

$$\begin{aligned} \left(v_{b_m}, d_{b_m}, h_{b_m}\right) &= \sum_{i=1}^{4} \left(v_{b_{mi}}, d_{b_{mi}}, h_{b_{mi}}\right) \frac{d^{i-1} u_{b_m}}{\mathrm{d}s^{i-1}} \\ &+ A_{b_m} \sum_{i=2}^{4} \left(v_{b_{mi}}^{(b)}, \mathrm{d}_{b_{mi}}^{(b)}, h_{b_{mi}}^{(b)}\right) \frac{d^{i-1} \mathcal{B}}{ds^{i-1}} \end{aligned} \tag{35}$$

where $A_{bm} = (-1)^m\, 4/M_B^2$ quantifies the decaying contribution of higher lateral Fourier modes, while $\sigma_{i_b}, p_{i_b}, v_{b_{mi}}, d_{b_{mi}}, h_{b_{mi}}, v_{b_{mi}}^{(b)}$, $d_{b_{mi}}^{(b)}$and $h_{b_{mi}}^{(b)}$ ,and are coefficients depending on the relevant physical parameters ( $\beta_u, \mathrm{d}_s, \tau_{*u}$)

[35] The nonhomogeneous, constant coefficient ordinary differential equation (34) can be solved in closed form by using the method of variation of parameters. Once the solution for $u_{b_m}$ is known, the remaining dependent variables can be solved in cascade for the $m$th Fourier mode simply by employing equation (35). The general solution of equation (34) reads

$$\begin{aligned} u_{b_m} &= \sum_{j=1}^{4} c_{b_{mj}}\, e^{\lambda_{b_{mj}} s} \\ &+ A_{b_m} \sum_{j=1}^{4} \left[\mathrm{g}_{b_{j0}} \int_0^s B(\xi)\, e^{\lambda_{b_{mj}}(s-\xi)}\, \mathrm{d}\xi + \mathrm{g}_{b_{j_1}} \mathcal{B}\right] \end{aligned} \tag{36}$$

where $\mathrm{g}_{b_{jk}}$ $(j = 1{,}4; k = 0{,}1)$ are constant coefficients depending on $\beta_{u,}\, d_{s,} \tau_{*u,}$ while $\lambda_{bmj}$ $(m = 1, \infty;\ j = 1{,}4)$are characteristic exponents for the $m$th lateral Fourier mode, and $c_{b_{mj}}$ $(j = 1{,}4)$ are integration constants to be specified on the basis of the boundary conditions at the channel ends. The long algebraic expressions of the various coefficients appearing in equations (34), (35), and (36) are reported in the Appendix, available as online supporting information.

[36] At a Wainganga section, the flow and bed topography are then affected not only by the local value of the width, accounted for through *B,* but also through the four convolution integrals, by the hydrodynamics and morphodynamics of the reaches located upstream (downstream influence) or downstream (upstream influence). This effect is analogous to that documented for the curvature forcing *[Lanzoni et al.,* 2006; *Frascati and Lanzoni,* 2009]).

### 3.2. The Linear Response Forced by Curvature

[37] The linear response of the flow field and of the bed configuration to the forcing induced by channel curvature is described by the $\mathcal{O}(v)$ nonhomogeneous linear differential problem:

$$\mathcal{L}\begin{pmatrix} u_c \\ v_c \\ d_c \\ h_c \end{pmatrix} = \begin{pmatrix} nb_1C \\ b_2C + b_3C' + b_4C'' \\ 0 \\ 0 \end{pmatrix} \tag{37}$$

satisfying the non-homogeneous boundary conditions

$$v_c = 0, \qquad (F_u^2 h_c - d_c)_{,n} = b_5 C + b_6\, C' \quad (n = \pm 1) \tag{38}$$

(38) where *C'* and *C″* are the first and second derivatives of the curvature.

[38] The problem presented by equations (37) and (38) governs the morphodynamics of constant width meandering rivers and is equivalent to that derived by *Zolezzi and Seminara* [2001]. By introducing the following Fourier expansions that satisfy the boundary conditions and respect the symmetric character of $v_c$ and the antisymmetric character of $u_c$, $d_c$, and $h_c$ typically associated with alternate channel bending, it can be transformed into a linear system of ordinary differential equations

$$\begin{aligned} u_c &= \sum_{m=0}^{\infty} u_{c_m} \sin(M_c n) \\ v_c &= \sum_{m=0}^{\infty} v_{c_m} \cos(M_c n) \\ d_c &= \left(\bar{h}_1 C + \bar{h}_2 C' + \bar{h}_3 C''\right) n + \sum_{m=0}^{\infty} d_{c_m} \sin(M_c n) \\ h_b &= \left(\bar{h}_1 C + \bar{h}_2 C' + \bar{h}_3 C''\right) n + \sum_{m=0}^{\infty} h_{c_m} \sin(M_c n) \end{aligned} \tag{39}$$

Where $M_c = (2m+1)\pi/2$ and

$$\begin{array}{llll} \bar{h}_1 & = b_2 & \bar{h}_2 = b_3 & \bar{h}_3 = b_5 \\ \bar{d}_1 = & F_0^2 \bar{h}_1 - b_4 & \bar{d}_2 = F_0^2 \bar{h}_2 - b_6 & \bar{d}_3 = F_0^2 \bar{h}_3 \end{array}$$

[39] The linear system of ordinary differential equations obtained by substituting expansions (39) into equations (37) and (38) can again be solved in closed form using the method of variation of parameters. In particular, the solution for $u_{c_m}$ reads

$$\begin{aligned} u_{c_m} &= \sum_{j=1}^{4} C_{c_m j}\, e^{\lambda_{c_m j} S} \\ &+ A_{c_m} \sum_{j=1}^{4} \left[ \mathrm{g}_{cf0} \int_0^S C(\xi) e^{\lambda_{c_m j}(S-\xi)} d\xi + \mathrm{g}_{cjl} C \right] \end{aligned} \tag{40}$$

where $\mathrm{g}_{cjk,}$ $\lambda_{c_m j}$ and $C_{c_m j}$ are analogous to the coefficients $\mathrm{g}_{bjk,}$ $\lambda_{b_m j}$, and $C_{b_m j}$ obtained by solving the problem forced by width variations. For the sake of completeness, also the algebraic expressions of

the various coefficients appearing in (39) and (40) are reported in the Appendix available as online supporting information. A comment is here worthwhile on the integration constants $C_{c_{mj}}$, reflecting the effects of the boundary conditions at the channel ends. Even though these constants can have a certain importance in the numerical simulations of the long-term river planform evolution *[Lanzoni and Seminara,* 2006], their influence on the flow field is local, owing to the rapid decay of the exponential functions they multiply. Therefore, both $C_{b_{mj}}$ and $C_{cmj}$ can be set to zero when calculating the equilibrium bed topography that establishes in a river reach for a given flow discharge.

### 3.3. Input Data and Applicability Conditions

[40] The mathematical model of Wainganga River is described so far can be easily implemented using the MATLAB language. Indeed, the analytical character of the solution implies a moderate computational effort. In particular, the input data needed for running the model consist of: (i) the spatial distributions of the channel axis and the river width, expressed in terms of the longitudinal curvilinear coordinate *s* and discretized by points (the discretization step being of the same order of magnitude of the average width); (ii) the water discharge conveyed by the river, $Q^*$*;* (iii) the average longitudinal bed slope of the considered river reach; and (iv) the characteristic sediment grain size, $d_s^*$ All these data allow one to determine univocally the dimensionless parameters used as input data to the model, namely the aspect ratio of the channel, $\beta_u = \beta_{avg}^* / D_u^*$ the dimensionless sediment grain size, $d_s = d_s^*/D_u^*$ the Shields parameter for the reference uniform flow, $\tau_{*_u}$; and the particle Reynolds number,$R_p$.

[41] The coordinates of the Wainganga River channel axis and the river banks need to be preliminarily processed in order to obtain the curvature and width distributions as a function of the intrinsic longitudinal coordinate *s.* These distributions are then smoothed with a Savitzky-Golay filter to avoid numerical problems in evaluating the derivatives. After the filtering, the points belonging to the bank and channel axis lines are remeshed, and the river width and curvature at every grid point are calculated. A low-pass band filter is finally applied in order to further smooth width and curvature variations and, hence, avoid spurious, high frequency fluctuations in the velocity field. After these preliminary procedures, the flow field (i.e., the velocity, the water elevation, the flow depth and, hence, the bed elevation) is calculated on a curvilinear two-dimensional grid (i.e, in the plane *s, n).*

[42] The definition of channel width requires some care. Indeed, the location of channel banks is easily identified and weakly stage dependent for canaliform rivers *[Br ce,* 1975]. Conversely, in the case of sinuous point Bar Rivers, the lateral bed profile at point bars is quite gentle, and hence, the channel width is stage dependent: small changes in water level cause relatively large changes in channel width. However, only the portion of the cross section where sediment transport occurs at formative conditions has to be accounted for when estimating the channel width relevant for morphological equilibrium *[Luch et al.,* 2012].

[43] Before examining the model, it is worthy to recall the conditions guaranteeing its applicability. First, the free vortex effect, whereby in a Bajrang ghat (Wainganga) meandering river, the maximum streamwise velocity alternates from one bank to the other, should be small. This requirement is satisfied if the bends are wide (small $\nu$), such that the longitudinal metric coefficient $N^{-1}$ does not differ significantly from one, and width variations are weak (small $\delta$). Second, the secondary flow induced by the topographic steering due to the bar-pool pattern should be small. This implies that the bends are long enough to ensure slow longitudinal variations of the flow field (small $\lambda_c$). Third, the intensity of the centrifugally driven secondary flow should be small, a condition that occurs for small values of the dimensionless group $\nu/\left(\beta_u\sqrt{C_{fu}}\right)$. Finally, the amplitude of bed perturbations should be small relatively to flow depth, for linearization to be valid. This condition is satisfied provided that the maximum value attained by $\nu\sqrt{\tau_{*_u}/C_{fu}}$ and $\lambda\beta_u\sqrt{\tau_{*_u}}$ is small enough *[Seminara and Solari,* 1998; *Bolla Pittaluga and Seminara,* 2011].

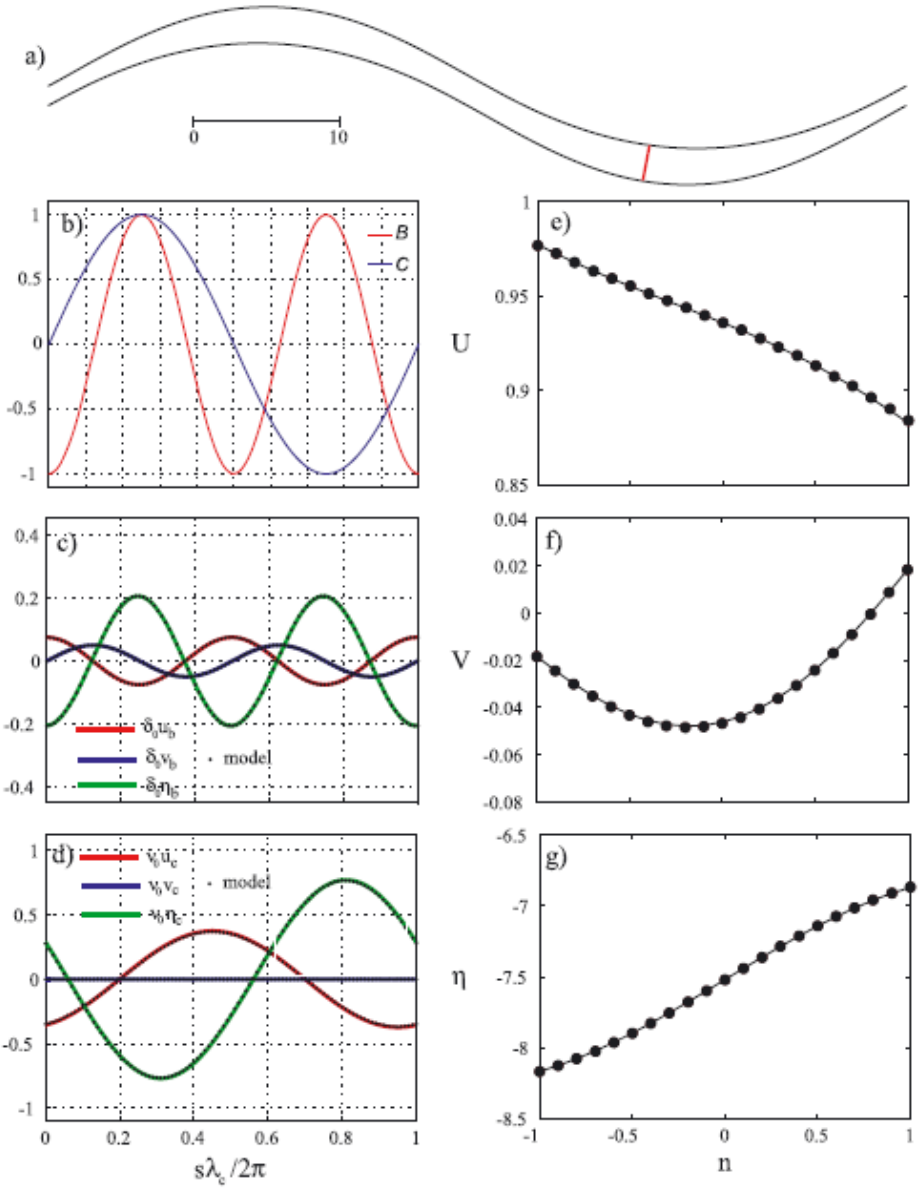


**Figure 4. (a) Planform configuration of a periodic sequence of sine generated meanders characterized by sinusoidal width variations. Solid red line shows the analyzed cross section. The planimetric scale is explained in terms of reach-averaged half-width units. (b) Streamwise distribution of $C$ and $B$. It has been assumed, without loss of generality, that channel width oscillates at double frequency with respect to channel curvature ($\lambda_b = 2\lambda_c$). (c and d) The longitudinal profiles of depth-averaged perturbation components induced by channel width and curvature variations, respectively, evaluated at the outer bank. (e-g) The cross-sectional distributions of the depth-averaged velocity components (U,V) and bed elevation $rj$. Solid lines are the periodic analytical solution provided by either *Blondeaux and Seminara* [1985] or *Repetto et al.* [2002], whereas black dots indicate the present theory. The values of the relevant dimen-sionless parameters are $\beta$= 12, $\tau *$=0.1, $d_s$ =0.01, $\nu$ = 0.05,$\delta$ = 0.25, $\lambda_c$= 0.1, $\lambda_b$= 0.2, plane bed. Flow is from left to right.**

### 3.4. Testing the Solution: Periodic Perturbations

[44] The theory presented here is quite general and applies to Wainganga meandering rivers characterized by irregular (not periodic) spatial distributions of channel axis curvature and cross-section width. However, to assess the reliability of the solution, we first consider the idealized case of a periodic sequence of small-amplitude meanders characterized by sinusoidal width variations. This schematic case

is described by the sum of (i) the $\mathcal{O}(v)$classical solution of *Blondeaux and Seminara* [1985] for constant width channels; and (ii) the $\mathcal{O}(\delta)$ depth-averaged solution of *Repetto et al.* [2002] for straight channels with periodic width variations.

[45] It is considered that the meandering planform shown in Figure 4a, in which the streamwise variations of curvature and width are described by the relations (Figure 4b):

$$C(s) = \exp(i2\pi\lambda_c S) + c.c \tag{41}$$

$$B(s) = exp(i2\pi\lambda_b s) + c.c. \tag{42}$$

where, $\lambda_c = B^*_{\text{avg}}/L^*_c$ and $\lambda_b = B^*_{\text{avg}}/L^*_b$ are meander and width variation wave numbers, $i$ is the imaginary unit, and *"c.c."* denotes the complex conjugate.

[46] Figures 4c-4g show the comparison between the analytical solutions of *Blondeaux and Seminara* [1985] and *Repetto et al.* [2002] and the present theory applied to the periodic planform depicted in Figure 4a. The overlap between the various solutions confirms the reliability of the present formulation. In order to obtain such accuracy, particular care has been devoted to the computation of the four convolution integrals, which appear in equations (36) and (40). Both the functions $C$ and $\mathcal{B}$ have been assumed to vary linearly between two consecutive nodes, and the integration has been performed by using a semianalytical approach. Moreover, taking advantage of the fact that the functions to be integrated decay exponentially, the integration has been truncated when the function is smaller than a given tolerance (say 0.0001), with a significant reduction of the computational time (see *Frascati and Lanzoni* [2009] for further details).

## 4. Comparison With Field Observations

[47] The performance of the model has been tested through a comparison with field observations, collected in a reach of the upper Wainganga River (Figure 5). The Wainganga river flows southward across the limit of Balaghat district through the floodplain; its length, from its Dam on Dhutighat to the south border of Balaghat district from where Wainganga river debouching into the Bhandara district of Maharastra , is about 98 km. Its drainage basin, including most of the Maikal ranges slopes, the upper Wainganga basin (Peninsular India). The Wainganga River presents a wide variety of morphological features along its path; including multi channel braided reaches and single thread meandering/sinuous reaches.

[48] The considered reach is about 41 km long, has an average width of 250 m, a tortuosity $\sigma_t = 1.23$, and an overall sinuosity lower than 1.5. The upstream section of the reach is located just before the confluence with the Sarrati stream. While the downstream section is located after the confluence with the Bagh and Bawanthadi rivers.. The average bed slope, estimated by least squares linear interpolation of the average bottom elevations calculated for 15 sections recently surveyed along the reach, is equal to 0.02% (Figure 6a).

[49] The low discharge river bed is composed by a bimodal mixture of sand and gravel (Figure 6b) with geometric mean grain size $\mathrm{d}^*_{sg} = 1.6$ mm. Thepresenceofthis mixture is strictly associated with the coarse sediment supply provided by the Chandan, Bagh and Bawanthadi rivers during floods events. These streams, in fact, due to their proximity to the Maikal Mountains, have a high longitudinal gradient and during flood events can transport relatively coarse material as suspended load. These coarser sediments then deposit on the finer bed sediments of the Wainganga River, owing to the lower flow strength characterizing it.

[50] Longitudinal river bank protection and groins are extensively present along the stream and strongly affect the river morphology, enhancing the incision of the river bed. The

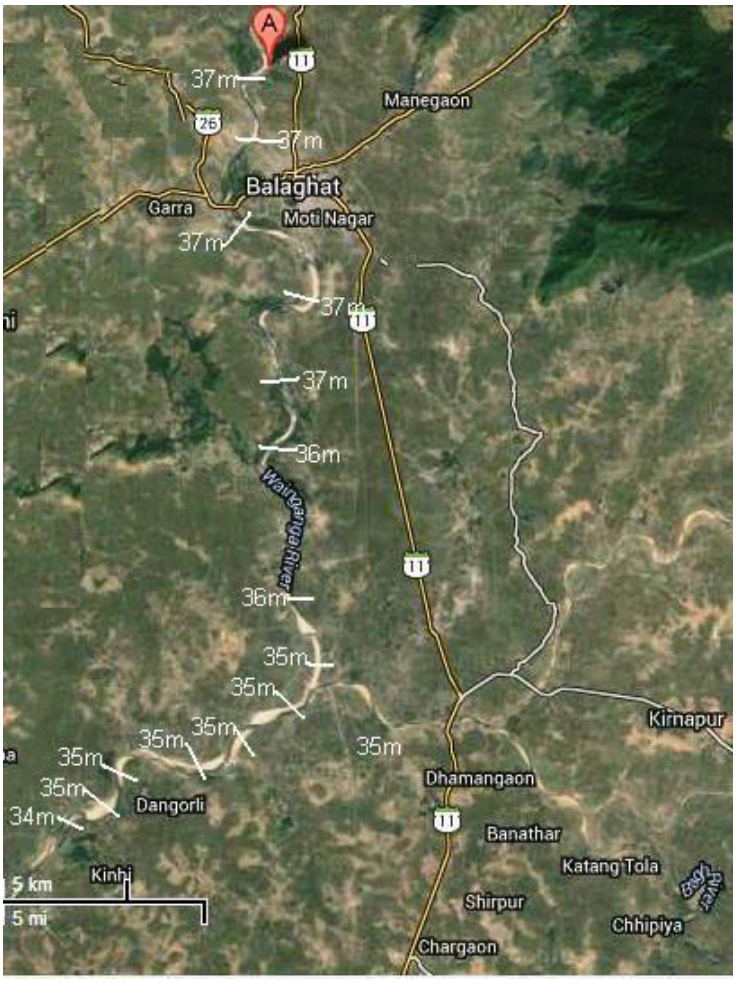


**Figure 5. Planform configuration of the investigated Wainganga river reach, including the confluences with the Bagh and Bawanthadi streams. The image has been downloaded from Google maps. The sections drawn in the figure are those recently surveyed by Dr N. L. Dongre (2014).The flow is from north to south.**

investigated reach is a typical example of a sinuous point bar river, with a single thread section (the active channel) flanked by wider expansion zones contained within the main river levees. The secondary banks delimiting the single thread section are made of varying grain size material, from coarse sand to silt and are protected except along the segments where the river is allowed to flood the adjacent storage zones. The bed forms within the active channel consist mainly of sandy point bars that are submerged for discharges above about 1000 - 1500 $m^3/s$. These bed forms appear to be remarkably stable: only some minor changes have been observed in the period 1982-2013, despite the occurrence of three major flood events. The longitudinal riverbank protection allows the inundation of adjacent expansion flood plains for a discharge of about 3000 $m^3/s$, corresponding to the ordinary flood, i.e., the discharge that is exceeded at least 10 days a year. Owing to the relevant incision experienced by this rivers reach, bankfull conditions are approached only during major, less frequent floods, for discharges of about 4000 - 5000 $m^3/s$. The bank-full stage then corresponds to the elevations of the main levees of the river.

[51] As discussed, the channel width relevant for Wainganga River morphological equilibrium has to be estimated with reference to the morphologically active part of the channel cross section, by neglecting the shallower cross-section regions where, under formative discharge conditions, no sediment transport occurs. It is then determined the single thread section width, excluding the expansion zones that are inundated for floods larger than the ordinary one and the region above the secondary banks. Figure 6c shows the along stream distributions of the channel active width extracted from the satellite image of

Figure 5 and the topographic and thematic maps provided by *Autoritd di Bacino del Fiume Po* [2009]. The dimensionless intensity of width variations takes the value $\delta$ = 0.761 while the curvature ratio is $v$ = 0.125. The mean value of the dimensionless intrinsic wave number is $\lambda_c$= 0.03, and hence, the bends can be considered long, i.e., the topographic component of the secondary flow, being of order $0(4\lambda_{cc})$ = 0.12, is weak.

[52] Sediment grain size and water discharge are two very major input requirements for the model. Their choice is not straightforward since the model does not account for graded sediment and for flow discharge variations observed during floods. Nevertheless, it is investigated the performance of the Wainganga River model by varying $d_s^*$ and $Q^*$ within physically plausible ranges, discussing whether the values ensuring the best fit with observed data from Wainganga River provide a reasonable description of the sediment bed composition and of the discharge responsible for shaping the surveyed bed topography.

[53] Figure 7 a longitudinal profile of Wainganga, Bagh and Bawanthadi River indicates the overall error along the investigated reach, computed as the mean of the absolute value of the differences between observed and calculated bed elevations. It appears that accounting for both curvature and width variation effects (white circles) invariably produces an improvement of the solution (i.e., a lower error). The uniform flow conditions yielding the lower values of e are as follows: $Q$ = 1550 m$^3$/s, $D_u^*$=4.5m, $U_U^*$ = 1.3 m/s, given a sediment grain size $d_s^*$ = 3 mm. The corresponding dimensionless input parameters are $\beta_u$= 29.8; $d_s$ = 0.00070; $\tau_{*_u}$=0.18; $R_p$ = 661. The parameter $v/\left(\beta\sqrt{C_{fu}}\right)$controlling the intensity of the centrifugally driven secondary flow, takes the value 0.057, implying mildly curved bends. Finally, the maximum value attained by the dimensionless groups $v\sqrt{\theta/}\sqrt{C_{fu}}$, and $\beta\sqrt{\theta\lambda_c}$ is 0.716 at the limit for applying a linearized model. We can then conclude that the river reach under investigation is characterized by wide (small $v$),

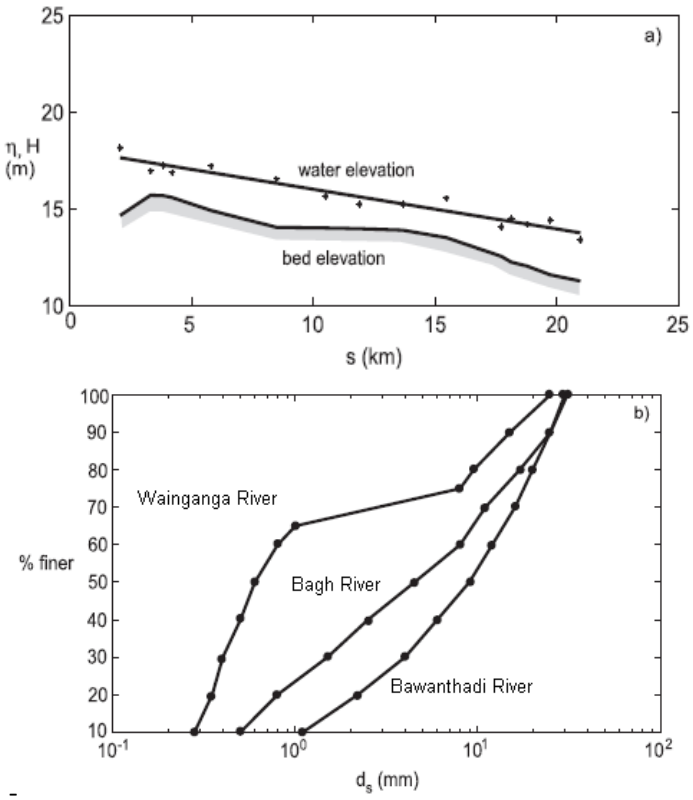

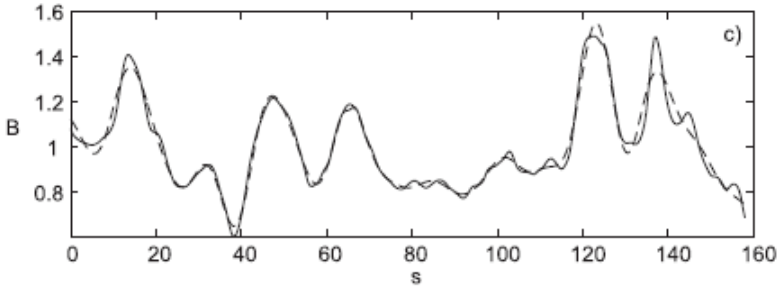


**Figure 6. (a) Longitudinal profiles of bed and water surface elevations. The former line is attained by considering the average bottom elevations of the cross sections surveyed by *Dr N.L.Dongre(2014)* along the reach. The water surface profile has been obtained by least square fitting the water surface elevations calculated running HEC-RAS under uniform flow conditions, assuming a relatively low water discharge (= 100 $m^3$ /s), such that only the active river bed is inundated by water flow. (b) Grain size distributions of the bed sediment in the investigated Wainganga River reach and in the two tributary streams, Bagh and Bawanthadi . (c) Longitudinal distribution of dimensionless active channel width *B* before (continuous line) and after (dashed line) the smoothing with a Savitzky-Golay filter, applied to avoid spurious, high frequency fluctuations in the velocity field**

mildly curved (small $v/\left(\beta\sqrt{C_{fu}}\right)$), and long (small $4\lambda_c$) bends in which nonlinear effects of bed perturbations can be reasonably neglected as a first approximation.

[54] The characteristic grain size eventually chosen in the simulation is very close, but slightly higher than the geometric mean grain size of the mixture (=1.6 mm). Although the geometric grain size has been found to be a useful quantity for describing the behavior of bimodal mixtures [see, e.g., *Lanzoni and Tubino,* 1999; *Lanzoni,* 2000], this result could be justified by the fact that the granulometric distribution of the investigated reach (as well as the flow resistance) is likely strongly influenced by the coarser sediment brought during flood events by the Bagh and Bawanthadi.

[55] The flow discharge (=1550 $m^3$/s) that ensures the best agreement between observed and calculated topography of Wainganga River is slightly larger than the discharge for which the point bars start to be submerged (~1000-1500 $m^3$/s) and is lower than both the ordinary flood discharge (~3000 $m^3$/s), for which the expansion areas adjacent to the main channel start to be flooded, and the bankfull discharge (~4000-5000 $m^3$/s). Also this result is reasonable. Experimental observations and common experience suggest that the river topography is usually determined by flood events of moderate intensity, which recur much more frequently, rather than by extreme floods *[Wolman and Miller,* 1960]. Strong morphological changes are likely affecting the river bed during flood events, acting on a time scale comparable with that of the flood. The theoretical and experimental analyses carried out by *Tubino* [1991] suggest that, under unsteady flow conditions, a damping of bar dimensions occurs during the rising of a flood while bar amplitude attains a maximum during the longer falling stage. A similar behavior has been documented by *Bolla Pittaluga and Seminara* [2011], who investigated the nonlinear response of the system as the externally imposed flood duration varies with respect to the morphological time scale. The maximum bed scour reached at dynamic equilibrium was found to be invariably lower than the steady value corresponding to peak discharge. Moreover, the maximum scour experienced at a particular location during the passage of the flood may be larger than the final equilibrium value owing to a temporal overshooting. These results suggest that a discharge smaller than the peak flood value should be con-sidered in order to predict the large scale bed form features observed when surveying a river bed. In the present case, the steady discharge ensuring the better agreement between predicted and observed bed topography is about half of the ordinary flood discharge, a reasonable result in view of the unsteady effects discussed above and the well known tendency of linearized model to overestimate the amplitude of bed topography.

[56] Figure 8 shows the comparison between the computed cross-section bed elevations and those resulting from the survey carried out by Dr. N L Dongre (2014). Note that the plots refer to the

perturbations of the bed elevation with respect to a hypothetical undisturbed sloping flat bed (i.e., the elevation due to the average slope is removed). Flood plains are excluded from this representation since, as mentioned above, the formative flow discharge is supposed to be constrained within the main river bed, owing to the diffuse presence of longitudinal bank protections. It appears that the overall agreement is remarkably good. Indeed, not only the maximum and minimum bed elevation within a cross section are generally reproduced, but also the alternating transverse bending of the river bed due to curvature and width variation forcing. This latter result can be better appreciated from the comparison reported in Figure 9, showing a color map of the computed bed topography along a portion of the investigated river reach and the corresponding aerial photo. In particular, channel width variations determine a generalized reduction of the scour and an enhanced deposition in the correspondence of the upstream bend, while just an opposite trend is exhibited by the relatively mild curve located in the second half of the reach (compare Figures 9a,9b,9c,9d,9e,9f,9g,and 9h).

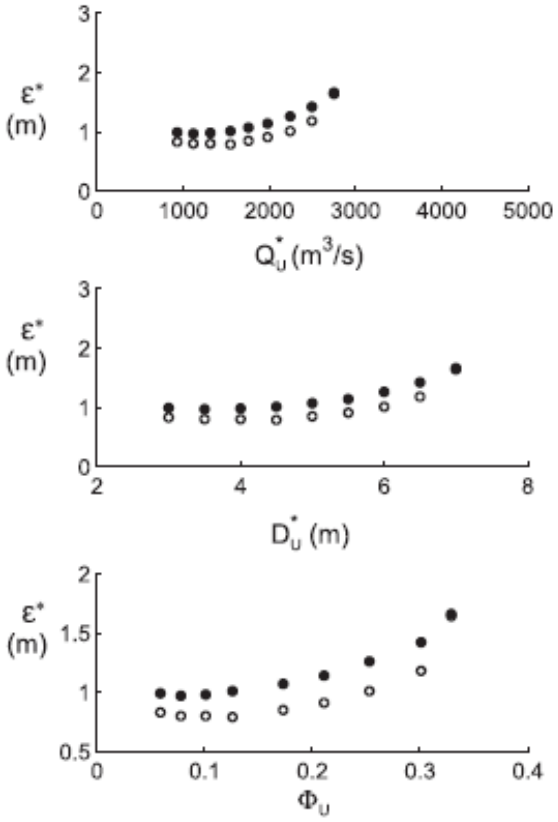


**Figure 7. The mean absolute error e along the investigated reach is plotted versus the water discharge *Q*, the uniform flow depth $D^*_u$ and the intensity $\Phi_u$ of uniform flow sediment transport. The error is computed as the difference between the bed elevations of the surveyed sections (Figure 5) and those calculated with the model. White circles denote the complete solution, including both curvature and width variations effects; black circles refer to the solution obtained by considering only the curvature forcing**

## 5. Discussion

[57] Considering the limitations inherent in linearization, it was shown that the present model can be also applied to rapidly assess the morphological tendencies of an alluvial river. The overall comparison with the bed topography observed in a typical reach of the Wainganga River (India) is quite good, provided that suitable values of the characteristic sediment bed size and the flow discharge (Dongra.N.L, 2014) are selected. It is then suggested that, after such a preliminary calibration, the model can be profitably used to investigate how the river bed topography likely reacts to changes in external forcing (e.g., variations in the hydrological regime) or in the river planform geometry (e.g., associated with engineering works or

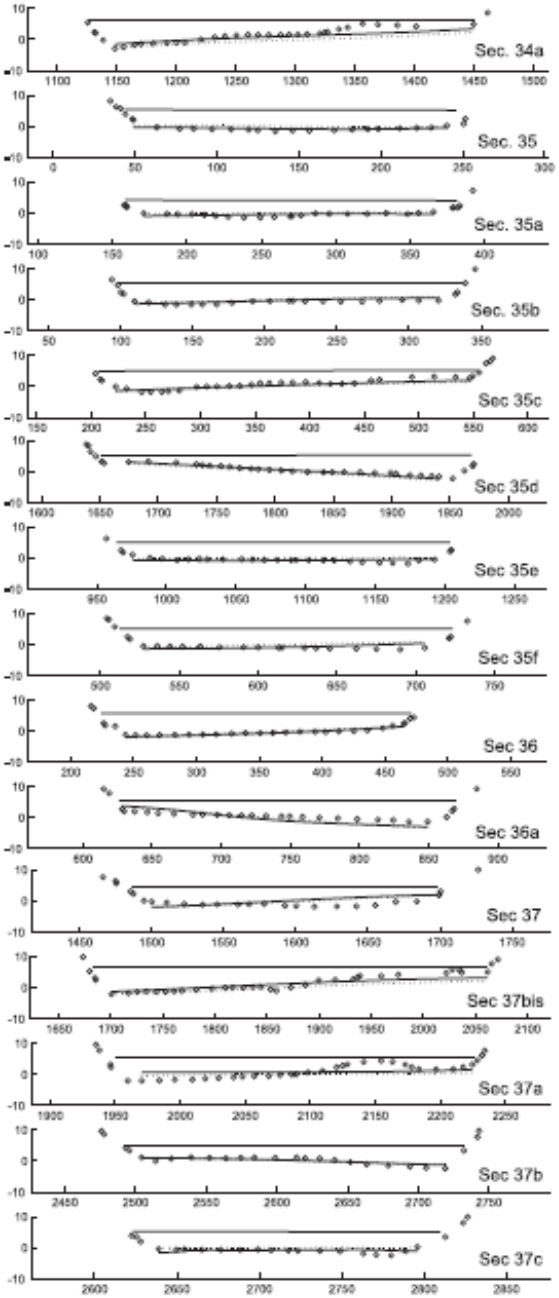


**Figure 8. Comparison between computed (continuous line) bed elevations and those measured (white circles) in the cross sections surveyed by Dr N.L.Dongre and shown in Figure 5. The complete solution (continuous line), including both curvature and width variations effects and the solution considering only curvature effects (dotted line) have been used for estimating the bed topography. The flow is entering into the plot plane, and the water surface for each section is represented by a horizontal line.**

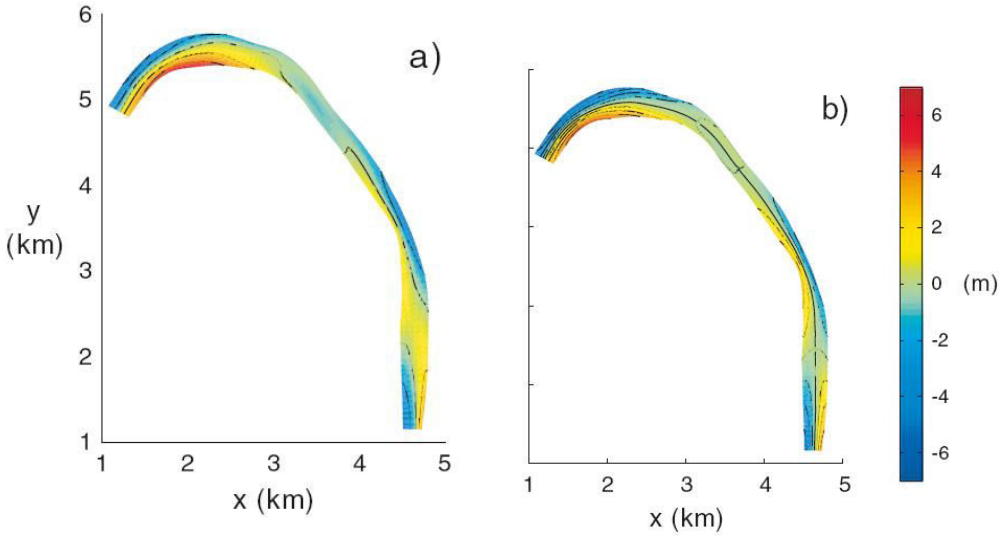
a)
b)
y (km)
x (km)
x (km)
(m)
6
4
2
0
-2
-4
-6

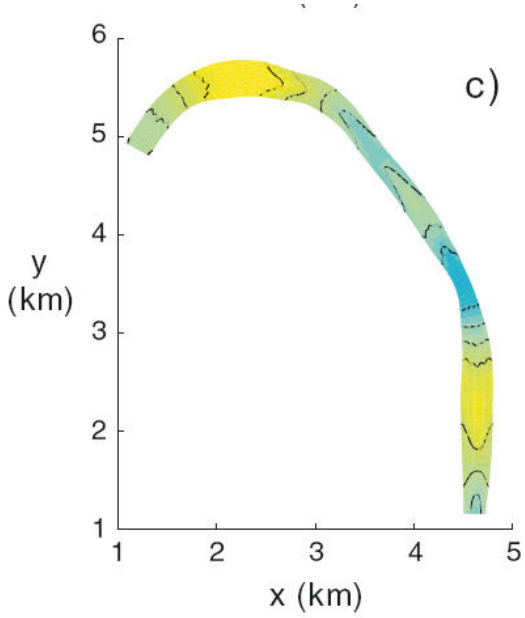
c)
y (km)
x (km)

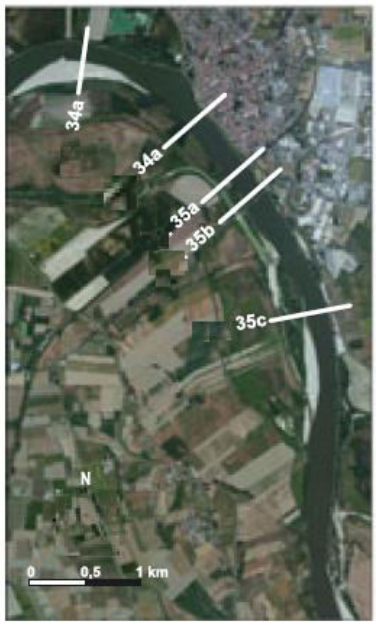
d)
34a
34a
35a
35b
35c
N
0
0,5
1 km

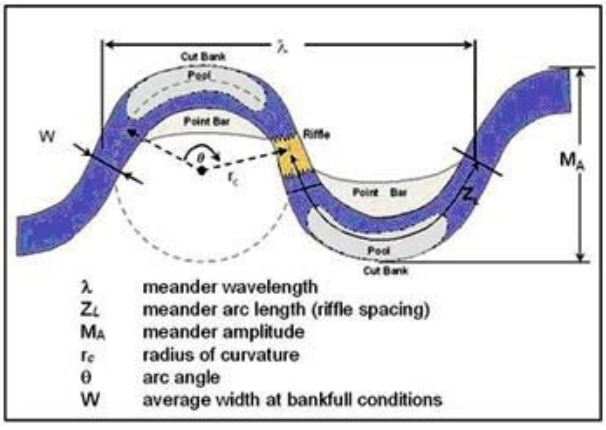
Cut Bank
Pool
Point Bar
Riffle
W
θ
$r_c$
Point Bar
Pool
Cut Bank
$M_A$
λ meander wavelength
$Z_L$ meander arc length (riffle spacing)
$M_A$ meander amplitude
$r_c$ radius of curvature
θ arc angle
W average width at bankfull conditions

e)

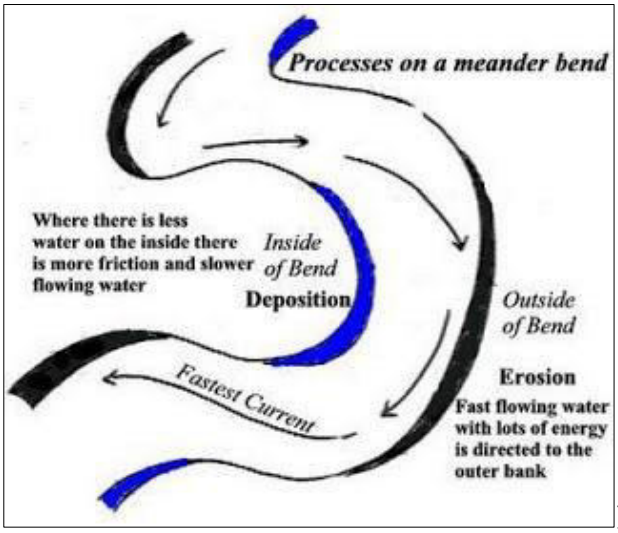
Processes on a meander bend
Where there is less water on the inside there is more friction and slower flowing water
Inside of Bend
Deposition
Outside of Bend
Erosion
Fast flowing water with lots of energy is directed to the outer bank
Fastest Current

f)

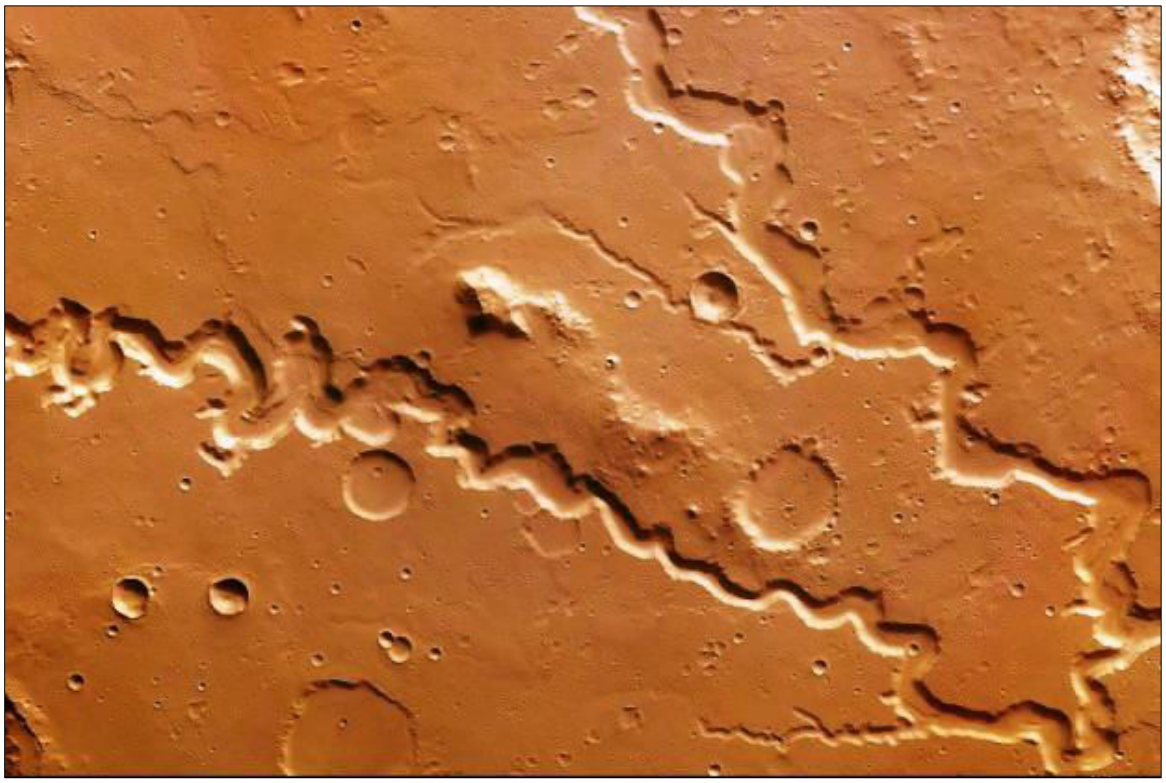

g)

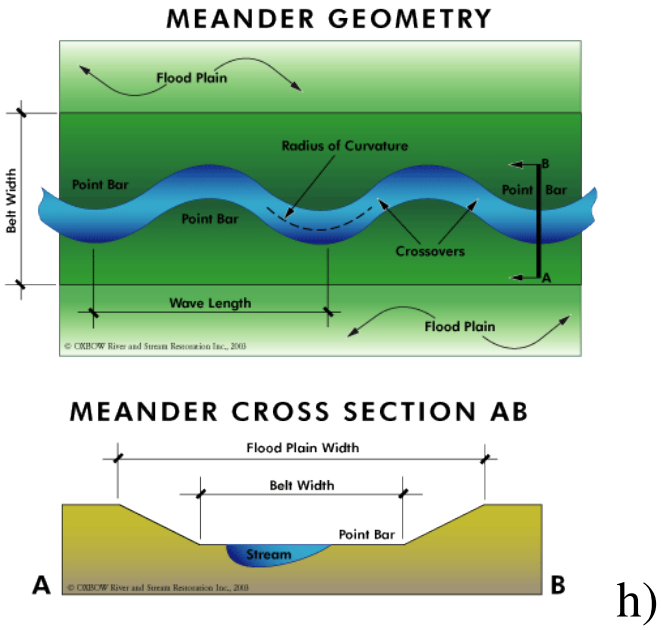


**Figure 9. (a) Bed topography of Wainganga River meandering resulting from the complete linear solution, including both the $O(\nu)$ and $O(\delta)$ contributions. (b) Bed topography accounting only for the $O(\nu)$ term due to curvature forcing. (c) Bed elevation changes associated with the $O(\delta)$contribution due to width variations effects. (d) Satellite image (from Google maps) of the specific portion of the river reach here considered and location of the surveyed sections. Flow is from top to bottom. (e)The Wainganga River at Dangorli shows the overall error along the investigated reach, computed as the mean of the absolute value of the difference between observed and calculated bed elevations (f)The Wainganga meandering near Bajrang Ghat, during survey it was recognized that the channel width relevant for morphological equilibrium has to be estimated with the active part of the channel and neglecting the shallower region under formative conditions, no sediment transport occurs (g) The complete linear response of the meandering river on Mars to spacing varying curvature and width exploiting the meandering river ability of the model similar to the morphological tendencies developed in the Wainganga River. (h) Showing generalized explanation of the natural tendency of running water to develop meander patterns in Wainganga River**

restoration activities). Indeed, the analytical character of the model, unlike the complete two-dimensional movable bed models, allows a fast recognition of the equilibrium configuration attained under given planform geometry, mean (Fig.9) bed slope, characteristic grain size, and formative flow discharge. Note that the analysis of the equilibrium configuration of a given river reach by using a complete two-dimensional mathematical model is not only extremely time consuming, since the equilibrium is attained only asymptotically, but is also likely influenced by the initial condition used for the bed topography.

[58] The sensitivity analysis carried out by varying the relevant dimensionless parameters (the width to depth ratio, $\beta$, the dimensionless grain size, $d_s$ and the Shields stress $\tau_{*_u}$) indicated that when the highest values of $Q^*$ or the lowest values of $d_s^*$ were employed, the maximum height of the sediment bars and the maximum scour underwent a generalized increase along the reach. On the other hand, the bed form position along the reach (i.e., the phase lag with respect to bend apex or to the location of the widest cross section) was only slightly influenced by the change of the input parameters within the investigated ranges.

[59] Clearly, the morphological tendencies of the river are predicted only qualitatively when the limits of applicability of the model are not satisfied. It is briefly recalled here that these intrinsic limitations. First of all, it relies on a linearized treatment of the governing equations, which take advantage of the relatively slow variations of channel axis curvature and of channel width often characterizing alluvial rivers. The model, hence, fails to describe the behavior of sharp bends. Moreover, even in the case of mild and long meanders typically exhibited by alluvial rivers, the finite size of bed perturbations should be accounted

for if the aspect ratio of the channel is sufficiently large and the Shields stress is not too small $\left(\beta\sqrt{\theta}\ \left(v_0/\beta\sqrt{C_{fu,}}\lambda\right) = 0(1)\right)$[Bolla *Pittaluga and Seminara,* 2011]. Second, the model does not account for flow unsteadiness typical of floods. This is an issue that should be investigated in the near future to clarify the possibility of modeling the morphological effects of variable hydraulic regime in terms of a formative discharge. Another restriction of the model is related to the uniform sediment assumption. The selective transport of sediment with different grain sizes and the resulting grain sorting patterns, in fact, can significantly affect the river morphology. The transport in suspension, not considered here, can be relevant as well. Finally, the river reach is assumed to be in equilibrium, i.e., no net erosion and deposition is assumed, and no sediments sources or sinks external to the system are considered.

## 6. Conclusions

[60] The main conclusions of this paper can be summarized as follows:

[61] It is developed that an analytical model yielding the linear response of Wainganga meandering river to spatial distributions of channel axis curvature and cross-section width that, as typically observed in nature, can vary irregularly, although maintaining small values of the dimensionless curvature ($v$)and the intensity of width oscillations ($\delta$). The model describes the linear combination of the laterally antisymmetric flow field and bed topography pattern typical of curvature-driven point bars ($\mathcal{O}(v)$solution), and the laterally symmetrical pattern resulting from central bars induced by width variations ($\mathcal{O}(\delta)$solution). Both patterns are fundamental in controlling the rate of outer bank erosion and of inner bank deposition and, hence, in ensuring a reliable and robust simulation of planform meander migration.

[62] The model has been found to provide a correct prediction of the river morphology in the presence of wide mildly curved and long bends, as well as weak width variations. Indeed, under these conditions the amplitude of bed deformations are small with respect to flow depth, thus allowing linearization. Moreover, mixed nonlinear interactions $\mathcal{O}(v\delta)$and $\mathcal{O}(v^2)$, determining how the alternate point bar pattern due to channel curvature is affected by width variations as well as by the dynamics of mid-channel bars in constant width curved channels, can be neglected. Similarly, local streamline curvature effects are likely to play a minor role in the parameterization of secondary flow effects, unless the bend is relatively narrow ($v = \mathcal{O}(1)$)

[63] The analytical character of the model guarantees a straightforward integration within the mathematical models used to simulate the long term planimetric evolution of meandering rivers, with only a small increase of the computational effort as compared to the linearized flow field models usually adopted.

## Appendix A: Derivation of Equations (2)-(6)

[64] In order to derive the governing equations (2)-(6), it is considered that the Reynolds averaged momentum and continuity equations for an incompressible steady flow, written with respect to the Cartesian coordinates x*, *y*, and* z'.Here *x*, y** is a horizontal plane and *z** coincides with the vertical pointing upward. Observing that in the investigated problem, the horizontal scale of the relevant hydrodynamic processes largely exceeds the flow depth, it can be assumed that the pressure is distributed hydrostatically along $z^*$ and replaces the pressure gradient with the slope of the free surface. Moreover, if the attention is restricted to the central part of the channel (neglecting the bank region), the slowly varying character of the flow field implies that the horizontal derivatives of the stress tensor can also be neglected. Further assuming a classical Boussinesq eddy-viscosity closure *[Tennekes andLumley,* 1972] for the remaining components of the additional Reynolds stresses, we obtain

$$uu_{,x} + vu_{,y} + wu_{,z} = -H,x + (v_T u, z), z$$
$$uv_{,x} + vv_{,y} + wu_{,z} = -H,y + (v_T v, z), z$$
$$u_{,x} + v_{,y} + w_{,z} = 0$$

where $H = F_u^2 D_u^* H^*$is the water surface elevation with respect to a given horizontal datum, $S_x$ and $S_y$ are the bed slopes in the $x$ and $y$ directions, and the normalized coordinates read $(x,y,z) = (x^*/B_{\mathrm{avg}}^* z^*/D_u^*)$

[65] In order to represent Wainganga a natural channel with curved alignment and variable width, it is then introduce the orthogonal curvilinear coordinate system depicted in Figure 2, such that $n$ is horizontal and $z$ points upward. However, while in Cartesian coordinates the differentials d$x$,d$y$,d$z$ correspond to distances measured along each of the three Cartesian coordinates axis, the analogous differentials in curvilinear coordinates do not necessarily have the same interpretation. Indeed, because of axis curvature, horizontal distances measured along different longitudinal coordinate surfaces are in general not equal when moving from one transverse coordinate surface to another. The metric coefficients $h_s$, $\mathrm{h_n}$,and $h_z$ account for this fact. In our case, $n$ and $z$ are rectilinear axis, and hence, $h_n = 1$, $h_z = \cos\theta \sim 1$ with $\theta$ is the angle that $z$ forms with the vertical. Recalling the expression for the various operators in orthogonal curvilinear coordinate (see, e.g., *Batchelor* [2000]), we eventually obtain the following:

$$\frac{uu_{,s}}{h_s} + vu_{,n} + wu_{,z} + \frac{vuh_{s,n}}{h_s} = -\frac{H,s}{h_s} + (v_T u,z),z$$

$$\frac{1}{h_s} uv_{,s} + v\, v_{,n} + wv_{,z} - \frac{1}{h_s} u^2 h_{s,n} = H,n + (v_T u,z),z$$

$$u_{,x} + (h_s v)_{,y} + (h_s w)_{,z} = 0$$

with $h_s = 1 + n^*/r^*(s^*) = 1 + v_0 nC$ . In order to obtain equations (2)-(4), we observe that $H^* = h^* - g^* S s^*$. Under uniform flow conditions, the channel axis slope is $S = C_{fu} F_u^2$ and, consequently, $H = h - \beta C_{fu} s$. We next must consider that the coordinate $n$ has been normalized with the local half channel width $B^*(s^*)$ and, hence, the following derivation chain rule has to be used:

$$\frac{\partial}{\partial \mathrm{s}} \rightarrow \frac{\partial}{\partial \mathrm{s}} + \mathrm{n}\frac{\mathrm{B,s}}{\mathrm{B}}\frac{\partial}{\partial \mathrm{n}}, \qquad \frac{\partial}{\partial \mathrm{n}} \rightarrow \frac{1}{\mathrm{B}}\frac{\partial}{\partial \mathrm{n}}$$

[66] The procedure followed to derive the Exner equation (5) is essentially similar to that leading to the continuity equation (4).

**Appendix B: Correction Due to Local Streamline Curvature Effect on Transverse Bed Shear Stress**

[67] The streamline curvature $C_s^*$ of the depth-averaged flow occurring in a curved channel can be expressed through the following dimensionless equation *[Mosselman,* 1998]:

$$vC_s = vC - \frac{V,s}{U}$$

where the second term on the right side accounts for the deviation of the streamline curvature from that of the stream-wise coordinate line that, in the present case, coincides with the channel axis. The effects of this term are of crucial importance when considering a straight channel subject to width variations *[Repetto et al.,* 2002]. Indeed, in this case $(C = 0)$, it is just the local streamline curvature that drives the secondary flow. In the case of a curved river reach of constant width, both the curvature of the channel axis and its correction due to the local streamline curvature deter-mine the intensity of the centrifugally driven secondary flow. Whether the former control prevails on the second (as is usu-ally assumed) depends on the parameter $v$. The effects of streamline curvature are likely important in narrow mean-dering bends ($v = \mathcal{O}(1)$where the free vortex mechanism, whereby the maximum streamwise velocity alternates from one bank to the other, is enhanced. For a given channel axis curvature, streamline curvature effects increase with chan-nel width; conversely, for a given channel width, they are enhanced as the channel axis curvature increases.

[68] An approximate assessment of these effects, involving a reasonable amount of algebra, can be obtained by including the streamline curvature in the term accounting for centrifugal effects on transverse bottom shear stress *[Repetto et al.,* 2002]. The quantity (20) then modifies as

$$\bar{V} = V + v\left[\frac{DU}{\beta_u\sqrt{C_{fu}}}\left(C - \frac{V,s}{U}\right)k_2 + \frac{D(DUC)_{,s}}{\beta_u^2 C_{fu}}k_3\right] \quad \text{(B1)}$$

[69] Recalling the expansions (25), it can be readily demonstrated that the operator $\mathcal{L}$ becomes

$$\mathcal{L}\begin{pmatrix} \left(\frac{\partial}{\partial_s} + a_1\right) & 0 & a_2 & \frac{\partial}{\partial_s} \\ 0 & \left(a_7\frac{\partial}{\partial_s} + a_3\right) & 0 & \frac{\partial}{\partial_n} \\ \frac{\partial}{\partial_s} & \frac{\partial}{\partial_n} & \frac{\partial}{\partial_s} & 0 \\ a_4\frac{\partial}{\partial_s} & \left(\frac{\partial}{\partial_n} + a_8\frac{\partial^2}{\partial n\,\partial s}\right) & \left(a_5\frac{\partial}{\partial_s} + a_6\frac{\partial^2}{\partial_{n^2}}\right) & -a_6F_u^2\frac{\partial^2}{\partial_{n^2}} \end{pmatrix} \quad \text{(B2)}$$

Where

$$a_7 = 1 - k_2\sqrt{C_{fu,}} \quad a_8 = -\frac{k_2}{\beta_u\sqrt{C_{fu}}} \quad \text{(B3)}$$

[70] The solution of the linearized flow field is formally equal to that already obtained in section 3.1 provided that the coefficients $a_4$, $a_5$, and $a_6$ are replaced by the following ones

$$\hat{a}_4 = a_4 + \frac{a_3a_8}{a_7}, \hat{a}_5 = a_5 + \frac{a_3a_8}{a_7}, \hat{a}_6 = a_6 + \frac{a_8}{F_u^2a_7},$$

[71] In the example of the Wainganga River here considered, the solution with the local streamline corrections implies only minor differences with respect to that obtained by simply considering the channel axis curvature.

**Appendix C:**

**C1. Coefficients of Equations (12)-(15)**

$$f_{10} = -nC\left(VU_{,n} + \beta_u\frac{\tau_s}{D}\right) - UVC - (k_0\Gamma_{n0} + k_1\Gamma_{n1})$$

$$f_{01} = nB_{,s}\left(UU_{,n} + H_{,n}\right) - \mathcal{B}\left(UU_{,s} + H_{,s} + \beta_u\frac{\tau_s}{D}\right)$$

$$g_{10} = nC\left(VV_{,,n} + H_{,n} + \beta_u\frac{\tau_n}{D}\right) + CU^2 - k_0(\Gamma_0 + \Gamma_{s^0}) - k_1(\Gamma_1 + \Gamma_{s1})$$

$$g_{01} = nB_{,s}UV_{,n} - \mathcal{B}\left(UV_{,s} + \beta_u\frac{\tau_n}{D}\right)$$

$$m_{10} = -C\left[n(DV)_{,n} + DV\right]$$

$$m_{01} = n\mathcal{B}_{,s}(DU)_{,n} - \mathcal{B}(DU)_{,}s$$

$$n_{10} = -C\left(q_n + nq_{n,n}\right)$$

$$n_{01} = n\mathcal{B}_{,s}q_{s,n} - \mathcal{B}_{qs,s}$$

where

$$\Gamma_{n0} = \frac{(D^2U^2C)_{,n}}{D\beta_u\sqrt{C_{fu}}} \qquad \Gamma_{n1} = \frac{\left[D^2U(UDC)_{,s}\right]_{,n}}{D\beta_u^2C_{fu}}$$

$$\Gamma_0 = 2\frac{(D^2UVC),n}{D\beta_u\sqrt{C_{fu}}} \qquad \Gamma_1 = 2\frac{\left[D^2V(UDC)_{,s}\right]_{,n}}{D\beta_u^2C_{fu}}$$

$$\Gamma_{s0} = \frac{(D^2U^2C)_{,s}}{D\beta_u\sqrt{C_{fu}}} \qquad \Gamma_{s1} = \frac{\left[D^2U(UDC)_{,s}\right]_{,s}}{D\beta_u^2 C_{fu}}$$

**C1. Coefficients of Equations (26)**

$$C_{f1} = C_T s_1 u_c + (C_D + C_T{}^{s_2})d_c$$
$$C_{f2} = C_T s_1 u_c + (C_D + C_T{}^{s_2})d_b$$
$$\tau_{*1} = s_1 u_c + s_2 d_c$$
$$\tau_{*2} = s_1 u_b + s_2 d_b$$
$$\Phi_1 = s_1 \Phi_T{}^{u_c} + (\Phi_D + \Phi_T{}^{s_2})d_c$$
$$\Phi_2 = s_1 \Phi_T{}^{u_b} + (\Phi_D + \Phi_T{}^{s_2})d_b$$

Where

$$s_1 = \frac{2}{1 - C_T} \quad s_2 = \frac{C_D}{1 - C_T}$$
$$C_T = \tau_{*u}\frac{C_{f,\tau*}|_u}{C_{fu}} \qquad C_D = \frac{C_{f,D}|_u}{C_{fu}}$$
$$\Phi_T = \tau_{*u}\frac{\Phi_{,\tau*}|_u}{\Phi_u} \quad \Phi_D = \frac{\Phi_{,D}|_u}{\Phi_u}$$

**C3. Coefficients of Equations (37), (38), and (29)**

$$a_1 = \frac{2\beta_u C_{fu}}{1 - C_T} \qquad a_2 = \beta_u C_{fu}\left(\frac{C_D}{1 - C_T} - 1\right)$$
$$a_3 = \beta_u C_{fu} = \; a_4 = \frac{2\Phi_T}{1 - C_T}$$
$$a_5 = \Phi_D + \frac{C_D\Phi_T}{1 - C_T} \quad a_6 = \frac{r}{\beta_u\sqrt{\tau_* u}}$$
$$a_7 = 1$$
$$b_1 = -\beta_u C_{fu} \qquad b_2 = 1 - \sqrt{C_{fu}k_2}$$
$$b_3 = -\frac{k_0}{\beta_u\sqrt{C_{fu}}} - \frac{k_3}{\beta}\, b_4 = -\frac{k_1}{\beta_u^2 C_{fu}}$$
$$b_5 = \frac{k_2\sqrt{\tau_* u}}{r\sqrt{C_{fu}}} \qquad b_6 = \frac{k_3\sqrt{\tau_{*u}}}{r\beta_u C_{fu}}$$

**Notations**

$a_i (i = 1,6)$constant coefficients
$B. B_{avg,} B_0$ local, average and maximum half channel width
$\mathcal{B}$ Dimensionless width perturbation
$b_i$ ($i$ = 1,6) constant coefficients
$C$ curvature of the channel axis
$C_f$,$C_{fu}$ local and uniform flow friction coefficient
$C_{fi}$($i$ = 1,2) constant coefficients
$c_{\text{bmj}}$, *ccmj* integration constants
$D$,$D_u$ local and uniform flow depth
$d_s$ sediment grain size
$\mathcal{F}$vertical distribution of the uniform flow with local flow characteristics
*Fu* Froude number of the uniform flow
$f_{ij}$ constant coefficients

$Gi$ vertical structure of the secondary flow due to channel axis curvature ($i$ = 0) and longitudinal convection ($i$ = 1)
$g$ gravitational constant
$g_{ij}$ constant coefficients
$g_{\mathrm{bjk}}$, $g_{\mathrm{cjk}}$ constant coefficients
$H$ local water surface elevation with respect to the horizontal plane containing n
$k$ von Karman constant
$k_i$ redistribution coefficients due to centrifugal ($i$ = 0,2) and convective ($i$ =1,3) secondary flow effects
$L$ length of the investigated river reache
$L_b$ wavelength of width variation perturbation
$L_c$ intrinsic meander wavelength
$\mathcal{L}, \mathcal{L}_b$ differential operators
$M_b$, $M_c$ periodicity coefficients
$m_{ij}$constant coefficients
$\mathcal{N}^{-1}$longitudinal metric coefficient
$\mathcal{N}$vertical distribution of the eddy viscosity
$n_{ij}$ constant coefficients
$q_s$, $q_n$ longitudinal and lateral components of the unit width sediment flux, $\mathbf{q}$
$R$ local radius of curvature of the channel axis
$R_0$ typical value of the radius of curvature
$R_p$ particle Reynolds number
$\mathbf{n}_b$ unit vector normal to the banks
$r$ empirical constant
$s$, $n$, $z$ intrinsic longitudinal, lateral and vertical coordinate, respectively
$U$, $V$ local values of depth-averaged longitudinal and transverse velocities, respectively
$U_{\mathrm{avg}}$ average depth-averaged velocity
$V$ depth-averaged transverse velocity accounting for secondary flow corrections in the bed shear stress
$u, v, w$longitudinal, lateral and vertical components of the local velocity, respectively
$u_b, v_b, d_b, h_b$ flow field perturbations due to width variations
$u_c, v_c, d_c, h_c$ flow field perturbations due to channel axis curvature
$\overline{v}$ local distribution of the centrifugally induced secondary flow
$x$ arbitrarily selected reference Cartesian axis
$z_0$reference level at which the no slip condition is applied
$\beta_u$ aspect ratio of the uniform flow
$\delta$ intensity of longitudinal width variations
$\eta$ local bed elevation
$\theta_c$angle between the channel axis and the $x$-direction
$\lambda_b$ wave number of channel width perturbations
$\lambda_c$intrinsic meander wave number
$\lambda_{bmj}, \lambda_{cmj}$characteristic exponents
$v$ curvature ratio
$v_T$turbulent eddy viscosity
$\xi$ normalized vertical coordinate
$\xi_0$ normalized reference level
$\rho, \rho_s$water and sediment density, respectively
$\rho_{bi}, \rho_{ci}$constant coefficients
$\sigma_{bi}, \sigma_{ci}$constant coefficients
$\tau_*, \tau_{*u}$local and uniform flow Shields stress
$\tau_{*i}(i = 1,2)$constant coefficientsr*s*,
$\tau_{\mathrm{s}}, \tau_{\mathrm{n}}$ longitudinal and transverse components of the bed shear stress, $\tau$

$\Phi, \Phi_u$ local and uniform flow intensity of sediment transport
$\Phi_i (i=1,2)$ constant coefficients

## References


- Allmendinger, N. E., J. E. Pizzuto, N. Potter Jr., T. E. Johnson, and W. Cully Hession (2005), The influence of riparian vegetation on stream width, eastern Pennsylvania, USA, *GSA Bulletin, 117*, 229-243, doi:10.1130/B25447.1.
- Batchelor, G. K. (2000), *An Introduction to Fluid Dynamics*, Cambridge,Univ. U. K.
- Blondeaux, P., and G. Seminara (1985), A unified bar-bend theory of river meanders, *J. FluidMech., 157,* 449-470.
- Bolla Pittaluga, M., and G. Seminara (2011), Nonlinearity and unsteadiness in river meandering: A review of progress in theory and modelling, *Earth Surf. Processes Landforms, 36*(1), 20-38, doi:10.1002/esp.2089.
- Bolla Pittaluga, M., G. Nobile, and G. Seminara (2009), A nonlinear model for river meandering, *Water Resour. Res., 45,* W04432, doi:10.1029/2008WR007298.
- Brice, J. C. (1975), Air photo interpretation of the form and behavior of alluvial rivers, Final Report to the U.S. Army Research Office-Durham, Wash. Univ., St. Louis, Mo., 10 pp.
- Brice, J. D. (1983), Factors in stability of relocated channels, *J Hydraul. Eng., 109*(10), 1298-1313.
- Camporeale, C., P. Perona, A. Porporato, and L. Ridolfi (2007), Hierarchy of models for meandering rivers and related mor-phodynamic processes, *Rev. Geophys., 45,* RG1001, doi:10.1029/2005RG000185.
- Chen, D., and J. Duan (2006), Modeling width adjustment in meandering channels, *J. Hydrol., 321,* 59-76.
- Crosato, A. (2007), Effects of smoothing and regridding in numerical meander migration models, *Water Resour. Res., 43,* W01401, doi:10.1029/2006WR005087.
- Darby, S. E., A. M. Alabyan, and M. J. Van de Wiel (2002), Numerical simulation of bank erosion and channel migration in meandering rivers, *Water Resour. Res., 38*(9), 1163, doi:10.1029/2001WR000602.
- Dean, R. B., (1974), Reynolds number dependence on skin friction in two-dimensional rectangular duct flow (Dongre NL, 2014) soand a discussion on the law of the Wake, *Aero Rep. 74-11,* Imperial Coll. London, London.
- Dongre N.L. (2014) The numerical modelling approach for the simulation of river meandering process in wainganga river Published in Google Mamagazine.
- Duan, J., and P. Julien (2005), Numerical simulation of the inception of channel meandering, *Earth Surf. Processes Landforms, 30,* 1093-1110, doi:10.1002/esp.1264.
- Einstein, A. H. (1950), The bedload function for sediment transport in open channel flow, *U.S. Dep. Agric. Tech. Bull. 1026,* Washington, D. C.
- Engelund, F., and E. Hansen (1967), *A Monograph on Sediment Transport in Alluvial Streams,* Dan. Tech. Press, Copenhagen.
- Federici, B., and C. Paola (2003), Dynamics of channel bifurcations in noncohesive sediments, *Water Resour. Res., 39*(6), 1162,doi:10.1029/2002WR001434.
- Frascati, A., and S. Lanzoni (2009), Morphodynamic regime and long-term evolution of meandering rivers, *J. Geophys. Res.* , *114,* F02002,doi:10.1029/2008JF001101.
- Frascati, A., and S. Lanzoni (2010), Long term river meandering as a part of chaotic dynamics? A contribution from mathematical modelling, *Earth Surf. Processes Landforms, 35,* 791-802, doi:10.1002/esp.1974.
- Hooke, J. M. (2007), Complexity, self-organisation and variation in behaviour in meandering rivers, *Geomorphology, 91* (3-4), 236-258, doi:10.1016/j.geomorph.2007.04.021.
- Howard, A. (1992), Modelling channel evolution and floodplain morphology, in *Floodplain Processes,* edited by M. G. Anderson, D. E. Walling, and P. D. Bates, 15-62, John Wiley, New York.
- Johannesson, H., and G. Parker (1989), Linear theory of river meanders, in *River Meandering, Water Resour. Monogr. Ser.* , vol. 12, edited by S. Ikeda and G. Parker, pp. 181-213, AGU, Washington D.C.
- Kalkwijk, J. P., and Th. H. J. De Vriend (1980), Computation of the flow in shallow river bends, *J. Hydraul. Res.*, *18,* 327-342.
- Lanzoni, S. (2000), Experiments on bar formation in a straight flume 2.
- Graded sediment, *Water Resour. Res., 36* (11), 3351-3363.
- Lanzoni, S., and M. Tubino (1999), Grain sorting and bar instability, *J. FluidMech., 393,* 149-174.
- Lanzoni, S., A. Siviglia, A. Frascati, and G. Seminara (2006), Long waves in erodible channels and morphodynamic influence, *Water Resour. Res., 42,* W06D17, doi:10.1029/2006WR004916

- Lanzoni, S., and G. Seminara (2006), On the nature of meander instability, *J. Geophys. Res., 111,* F04006, doi:10.1029/2005JF000416.
- Luchi, R., J. M. Hooke, G. Zolezzi, and W. Bertoldi (2010), Width variations and mid-channel bar inception in meanders: RiverBollin (UK), *Geomorphology, 119*(1-2), 1-8, doi:10.1016/j.geomorph. 2010.01.010.
- Luchi, R., G. Zolezzi, and M. Tubino (2011), Bend theory of river meanders with spatial width variations, *J. Fluid Mech., 681,* 311-339, doi:10.1017/jfm.2011.200.
- Luchi, R., M. Bolla Pittaluga, and G. Seminara (2012), Spatial width oscillations in meandering rivers at equilibrium, *Water Resour. Res., 48,* W05551, doi:10.1029/2011WR011117.
- Mosselman, E. (1998), Morphological modelling of rivers with erodible banks, *Hydrol. Processes, 12,* 1357-1370.
- Motta, D., J. D. Abad, E. J. Langendoen, and M. H. Garcia (2012), A simplified 2D model for meander migration with physically-based bank evolution, *Geomorphology, 163-164,* 10-25, doi:10.1016/ j.geomorph.2011.06.036.
- Parker, G., G. Seminara, and L. Solari (2003), Bed load at low Shields stress on arbitrarily sloping beds: Alternative entrainment formulation, *Water Resour. Res., 39*(7), 1183, doi:10.1029/2001WR001253.
- Parker, G., Y. Shimizu, G. V. Wilkerson, E. C. Eke, J. D. Abad, J. W. Lauer, C. Paola, W. E. Dietrich, and V. R. Voller (2011), A new framework for modeling the migration of meandering rivers, *Earth Surf. Processes Landforms, 36,* 70-86, doi:10.1002/esp.2113.
- Repetto, R., M. Tubino, and C. Paola (2002), Planimetric instability of channels with variable width, *J. Fluid Mech.*, 457, 79-109.
- Routher, N., and N. Olsen (2007), Modelling free-forming meander evolution in a laboratory channel using three-dimensional computational fluid dynamics, *Geomorphology, 89,* 308-319, doi:10.1016/j.geomorph.2006.12.009.
- Seminara, G. (2006), Meanders, *J. Fluid Mech.*, 554, 271-297.
- Seminara, G. (1998), Stability and morphodynamics, *Meccanica, 33,*59-99.
- Seminara, G., and L. Solari (1998), Finite amplitude bed deformations in totally and partially transporting wide channel bends, *Water Resour. Res.,* 34, 1585-1594.
- Smith, J. D., and S. R. McLean (1984), A model for flow in meandering streams, *Water Resour. Res.*, 20, 1301-1315.
- Solari, L., and G. Seminara (2005), On width variations in river meanders, *paper presented at RCEM2005 Conference, Int. Assoc. for Hydro- Environ. Eng. and Res.* , Urbana, Ill., 4-7 Oct
- Sun, T., P. Meaking, T. Jossang, andK. Schwarz(1996), Asimulationmodel for meandering rivers, *Water Resour. Res., 32*(9), 2937-2954.
- Talmon, A. M., N. Struiksma, and M. C. L. M. V. Mierlo (1995), Laboratory measurements of the sediment transport on transverse alluvial-bed slopes, *J. Hydraul. Res., 33,* 495-517.
- Tennekes, H., and J. L. Lumley (1972), *A First Course in Turbulence*,MIT Press, Cambridge, Mass.
- Transportation Research Board of the National Academies (2004), *Methodology for predicting channel migration,* NCHRP Web-Only Doc. 67 (Project 24-16), Washington, D. C. [Available at
- Tubino, M. (1991), Growth of alternate bars in unsteady flows, *Water. Resour. Res.,* 27(1), 37-52.
- Wolman, M. G., andJ. P. Miller(1960), Magnitude andfrequencyofforces in geomorphic processes, *J. Geol., 68,* 54-74.
- Wong, M., and G. Parker (2006), Reanalysis and correction of bed-loadrelation of Meyer-Peter and Muller using their own database, *J. Hydraul.*
- *Eng., 132,* 1159-1168.
- Zolezzi, G., and G. Seminara (2001), Downstream and upstream influence in river meandering. Part 1. General theory and application to overdeepening, *J. Fluid Mech.*, 438, 183-211.
- Zolezzi, G., R. Luchi, and M. Tubino (2012), Modeling morphodynamic processes in meandering rivers with spatial width variations, *Rev. Geo-phys., 50,* RG4005, doi:10.1029/2012RG000392.


---